CHAPTER 6

Ship Maneuvering

Chapter Outline

6.1. Introduction

Ship maneuvering comprises:

- course keeping (this concerns only the direction of the ship's longitudinal axis);
- course changing;
- track keeping (important in restricted waters);
- speed changing (especially stopping).

Maneuvering requirements are a standard part of the contract between shipyard and shipowner. IMO regulations specify minimum requirements for all ships, but shipowners may introduce

Practical Ship Hydrodynamics. DOI: 10.1016/B978-0-08-097150-6.10006-5

additional or more severe requirements for certain ship types, e.g. tugs, ferries, dredgers, exploration ships. Important questions for the specification of ship maneuverability may include:

- Does the ship keep a reasonably straight course (in autopilot or manual mode)?
- Under what conditions (current, wind) can the ship berth without tug assistance?
- Up to what ratio of wind speed to ship speed can the ship still be kept on all courses?
- Can the ship lay rudder in acceptable time from one side to the other?

Ship maneuverability is described by the following main characteristics:

- initial turning ability: ability to initiate a turn (rather quickly);
- sustained turning ability: ability for sustained (rather high) turning speed;
- yaw checking ability: ability to stop turning motion (rather quickly);
- stopping ability: ability to stop (in rather short distance and time);
- yaw stability: ability to move straight ahead in the absence of external disturbances (e.g. wind) at one rudder angle (so-called neutral rudder angle).

The sustained turning ability appears to be the least important, since it describes the ship behavior only for a time long after initiating a maneuver. The stopping ability is of interest only for slow speeds. For avoiding obstacles at high ship speed, it is far more effective to change course than to stop. (Course changes require less distance than stopping maneuvers for full speed.)

Understanding ship maneuvering and the related numerical and experimental tools is important for the designer for the choice of maneuvering equipment of a ship. Items of the maneuvering equipment may be:

- rudders;
- fixed fins (e.g. above the rudder; skeg);
- jet thrusters;
- propellers (including fixed pitch, controllable pitch, slewable, and cycloidal (e.g. Voith–Schneider propellers);
- adjustable ducts for propellers, steering nozzles;
- waterjets.

Both maneuvering and seakeeping of ships concern time-dependent ship motions, albeit with some differences:

- The main difficulty in both fields is to determine the fluid forces on the hull (including propeller and rudder) due to ship motions (and possibly waves).
- At least a primitive model of the maneuvering forces and motions should be part of any seakeeping simulation in oblique waves.

- Contrary to seakeeping, maneuvering is often investigated in shallow (and usually calm) water and sometimes in channels.
- Linear relations between velocities and forces are reasonable approximations for many applications in seakeeping; in maneuvering they are applicable only for rudder angles of a few degrees. This is one reason for the following differences.
- Seakeeping is mostly investigated in the frequency domain; maneuvering investigations employ time-domain simulations.
- In seakeeping, motion equations are written in an inertial coordinate system; in maneuvering simulations a ship-fixed system is applied. (This system, however, typically does not follow heel motions.)
- For fluid forces, viscosity is usually assumed to be of minor importance in seakeeping computations. In maneuvering simulations, the free surface is often neglected. Ideally, both free surface and viscous effects should be considered for both seakeeping and maneuvering.

Here we will focus on the most common computational methods for manoeuvring flows. Far more details, especially on maneuvering devices, can be found in Brix (1993).

6.2. Simulation of Maneuvering with Known Coefficients

6.2.1. Introduction and Definitions

The hydrodynamic forces of main interest in maneuvering are:

- the longitudinal force (resistance) X;
- the transverse force Y;
- the yaw moment N;

depending primarily on:

- the longitudinal speed u and acceleration $\dot{u}$;
- transverse speed v at midship section and acceleration $\dot{v}$;
- yaw rate (rate of rotation) $r = \dot{\psi}$ (rad/time) and yaw acceleration $\dot{r} = \ddot{\psi}$, where ψ is the yaw angle;
- the rudder angle δ (positive to port).

For heel angles exceeding approximately 10°, these relations are influenced substantially by heel. The heel may be caused by wind or, for Froude numbers exceeding approximately 0.25, by the maneuvering motions themselves. Thus at least for fast ships we are also interested in:

- the heeling moment K;
- the heel angle ϕ.

For scaling these forces and moments from model to full scale, or for estimating them from results in similar ships, *X, Y, K*, and *N* are made non-dimensional in one of the following ways:

$$\begin{Bmatrix} X' \\ Y' \\ K' \\ N' \end{Bmatrix} = \frac{1}{q \cdot L^2} \begin{Bmatrix} X \\ Y \\ K/L \\ N/L \end{Bmatrix} \quad \text{or} \quad \begin{Bmatrix} C_X \\ C_Y \\ C_K \\ C_N \end{Bmatrix} = \frac{1}{q \cdot L \cdot T} \begin{Bmatrix} X \\ Y \\ K/L \\ N/L \end{Bmatrix} \tag{6.1}$$

with $q = \rho \cdot u^2/2$ and ρ water density. Note that here we use the instantaneous longitudinal speed u (for $u \neq 0$) as reference speed. Alternatively, the ship speed at the beginning of the maneuver may be used as reference speed. L is the length between perpendiculars. The term 'forces' will from now on include both forces and moments, unless otherwise stated.

The motion velocities and accelerations are also made non-dimensional by suitable powers of u and L:

$$v' = v/u\,; \quad r' = r \cdot L/u\,; \quad \dot{u}' = \dot{u} \cdot L/u^2\,; \quad \dot{v}' = \dot{v} \cdot L/u^2\,; \quad \dot{r}' = \dot{r} \cdot L^2/u^2 \tag{6.2}$$

6.2.2. Force Coefficients

CFD or model tests may be used to determine the force coefficients. Then the body forces may be approximated by expressions like:

$$\begin{aligned} Y' = {} & Y_{\dot{v}}' \cdot \dot{v}' + Y_{\dot{r}}' \cdot \dot{r}' + Y_v' \cdot v' + Y_{v^3}' \cdot (v')^3 + Y_{vr^2}' \cdot v'(r')^2 + Y_{v\delta^2}' \cdot v'\delta^2 + Y_r' \cdot r' \\ & + Y_{r^3}' \cdot (r')^3 + \ldots \end{aligned} \tag{6.3}$$

$Y_{\dot{v}}'\ldots$ are non-dimensional coefficients. Unlike the above formula, such expressions may also involve terms like $Y_{ru}' \cdot r' \cdot \Delta u'$, where $\Delta u' = (u - V)/u$. V is a reference speed, normally the speed at the beginning of the maneuver. Comprehensive tables of such coefficients have been published, e.g. Wolff (1981) for models of five ship types (tanker, Series 60 $C_B = 0.7$, mariner, container ship, ferry) (Tables 6.1 and 6.2). The coefficients for u are based on $\Delta u = u - V$ in these tables. Corresponding to the small Froude numbers, the values do not contain heeling moments and the dependency of coefficients on heel angle. Such tables, together with the formulae for *X, Y*, and *N* as given above, may be used for time simulations of motions of such ships for an arbitrary time history of the rudder angle.

Wolff's results are deemed to be more reliable than other experimental results because they were obtained in large-amplitude, long-period motions of relatively large models (L between 6.4 and 8.7 m). Good accuracy in predicting the maneuvers of sharp single-screw ships in full scale from coefficients obtained from experiments with such models has been demonstrated. For full ships, for twin-screw ships, and for small models, substantial differences between model and full-scale maneuvering motions are observed. Correction methods from model to full scale need still further improvement.

Table 6.1: Data of four models used in maneuvering experiments (Wolff 1981)

	Tanker	Series 60	Container	Ferry
Scale	1:35	1:26	1:34	1:16
L_{pp}	8.286 m	7.034 m	8.029 m	8.725 m
B	1.357 m	1.005 m	0.947 m	1.048 m
T_{fp}	0.463 m	0.402 m	0.359 m	0.369 m
T_m	0.459 m	0.402 m	0.359 m	0.369 m
T_{ap}	0.456 m	0.402 m	0.359 m	0.369 m
C_B	0.805	0.700	0.604	0.644
Coord. origin aft of FP	4.143 m	3.517 m	4.014 m	4.362 m
LCG (x_G)	−0.270 m	0.035 m	−0.160 m	−0.149 m
Radius of gyration i_z	1.900 m	1.580 m	1.820 m	1.890 m
No. of propellers	1	1	2	2
Propeller turning	Right	Right	Outward	Outward
Propeller diameter	0.226 m	0.279 m	0.181 m	0.215 m
Propeller P/D	0.745	1.012	1.200	1.135
Propeller A_E/A_0	0.60	0.50	0.86	0.52
No. of blades	5	4	5	4

For small deviations of the ship from a straight path, only linear terms in the expressions for the forces need to be retained. In addition we neglect heel and all those terms that vanish for symmetrical ships to obtain the equations of motion:

$$(X'_{\dot{u}} - m')\dot{u}' + X'_u \Delta u' + X'_n \Delta n' = 0 \tag{6.4}$$

$$(Y'_{\dot{v}} - m')\dot{v}' + (Y'_{\dot{r}} - m'x'_G)\dot{r}' + Y'_v v' + (Y'_r - m')r' = -Y'_\delta \delta \tag{6.5}$$

$$(N'_{\dot{v}} - m'x'_G)\dot{v}' + (N'_{\dot{r}} - I'_{zz})\dot{r}' + N'_v v' + N'_v v' + (N'_r - m'x'_G)r = -N'_\delta \delta \tag{6.6}$$

I_{zz} is the moment of inertia with respect to the z-axis:

$$I_{zz} = \int (x^2 + y^2)\, \mathrm{d}m \tag{6.7}$$

$m' = m/(\frac{1}{2}\rho L^3)$ is the non-dimensional mass, $I'_{zz} = I_{zz}/(\frac{1}{2}\rho L^5)$ the non-dimensional moment of inertia coefficient.

If we just consider the linearized equations for side forces and yaw moments, we may write:

$$M'\dot{\vec{u}}' + D'\vec{u}' = \vec{r}'\Delta \tag{6.8}$$

with:

$$M' = \begin{bmatrix} -Y'_{\dot{v}} + m' & -Y_{\dot{r}}' + m'x'_G \\ -N'_{\dot{v}} + m'x'_G & -N'_{\dot{r}} + I'_{zz} \end{bmatrix};\ \vec{u}' = \begin{Bmatrix} v' \\ r' \end{Bmatrix} \tag{6.9}$$

$$D' = \begin{bmatrix} -Y'_v & -Y'_r + m' \\ -N'_v & -N'_r + m'x'_G \end{bmatrix}; \quad \vec{r}' = \begin{Bmatrix} Y'_\delta \\ N'_\delta \end{Bmatrix} \tag{6.10}$$

M' is the mass matrix, D' the damping matrix, $\vec{r}'$ the rudder effectiveness vector, and $\vec{u}'$ the motion vector. The terms on the right-hand side thus describe the steering action of the rudder. Some modifications of the above equation of motion are of interest:

1. If in addition a side thruster at location x_t is active with thrust T, the (non-dimensional) equation of motion modifies to:

$$M'\dot{\vec{u}}' + D'\vec{u}' = \vec{r}'\Delta + \begin{Bmatrix} T' \\ T'x'_t \end{Bmatrix} \tag{6.11}$$

Table 6.2: Non-dimensional hydrodynamic coefficients of four ship models (Wolff 1981); values to be multiplied by 10^{-6}

Model of / *Initial F_n*	*Tanker* 0.145	*Series 60* 0.200	*Container* 0.159	*Ferry* 0.278
m'	14 622	11 432	6 399	6 765
$x'_G m'$	365	57	−127	−116
I'_{zz}	766	573	329	319
$X'_{\dot{v}\dot{r}}$	−1 077	−1 064	0	0
$X'_{\dot{u}}$	−5 284	0	0	0
$X'_{\dot{u}u^2}$	−2 217	−2 559	−1 320	−4 336
X'_u	1 510	0	1 179	−2 355
X'_{u^2}	0	−2 851	0	−2 594
X'_{u^3}	−889	−3 908	−1 355	−3 279
X'_{v^2}	237	−838	−151	−571
X'_{r^2}	−1 598	−1 346	−696	−2 879
X'_{δ^2}	0	−1 833	−2 463	−2 559
X'_{v^2u}	2 001	2 536	0	3 425
X'_{δ^2u}	0	0	−470	−734
X'_{r^2u}	9 478	7 170	3 175	4 627
X'_{vr}	1 017	942	611	877
$X'_{v\delta}$	−482	−372	−340	−351
$X'_{r\delta}$	745	0	0	0
X'_{vu}	0	0	−207	0
X'_{vu^2}	0	−270	0	0
X'_{ru}	48	0	0	−19
X'_r	166	0	0	0
X'_δ	0	150	0	0
$X'_{\delta u^2}$	−4 717	0	0	0
$X'_{v^2\delta}$	−365	0	0	0
$X'_{r^2\delta}$	1 164	2 143	0	0
X'_{v^3}	−118	0	0	0
X'_{r^3}	−278	0	0	0
X'_{δ^3u}	0	621	213	2 185
X'_{δ^4}	0	0	−3 865	0
X'_{v^3u}	0	0	−447	0
X'_{r^3u}				

Model of	*Tanker*	*Series 60*	*Container*	*Ferry*
$Y'_{\dot{v}}$	−11 420	−12 608	−6 755	−7 396
$Y'_{\dot{v}v^2}$	−21 560	−34 899	−10 301	0
$Y'_{\dot{r}}$	−714	−771	−222	−600
$Y'_{\dot{r}r^2}$	−468	166	−63	0
Y'_0	−244	26	0	0
Y'_u	263	−69	−33	57
Y'_v	−15 338	−16 630	−8 470	−12 095
Y'_{v^3}	−36 832	−45 034	0	−137 302
Y'_{vr^2}	−19 040	−37 169	−31 214	−44 365
$Y'_{v\delta^2}$	0	0	−4 668	2 199
Y'_r	4 842	4 330	2 840	1 901
Y'_{r^2}	0	152	85	0
Y'_{r^3}	1 989	2 423	−1 945	−1 361
Y'_{ru}	0	−1 305	2 430	−1 297
Y'_{ru^2}	0	0	4 769	0
Y'_{rv^2}	22 878	10 230	−33 237	−36 490
$Y'_{r\delta^2}$	1 492	0	0	−2 752
Y'_δ	3 168	2 959	1 660	3 587
Y'_{δ^2}	0	0	0	98
Y'_{δ^3}	3 621	−7 494	0	0
Y'_{δ^4}	1 552	613	−99	0
Y'_{δ^5}	−5 526	4 344	−1 277	−6 262
$Y'_{\delta v^2}$	0	0	13 962	0
$Y'_{\delta r^2}$	1 637	0	2 438	0
$Y'_{\delta u}$	−4 562	−4 096	0	−5 096
$Y'_{\delta u^2}$	0	974	0	0
$Y'_{\delta^3 u}$	2 640	4 001	0	3 192
$Y'_{v\|v\|}$	−11 513	−19 989	−47 566	0
$Y'_{r\|r\|}$	−351	0	1 731	0
$Y'_{\delta\|\delta\|}$	−889	2 029	0	0
$Y'_{v^3 r}$	12 398	0	0	0
$Y'_{r^3 u}$	0	2 070	0	0

TABLE 6.2 continued

Model of	*Tanker*	*Series 60*	*Container*	*Ferry*
$N'_{\dot{v}}$	−523	326	239	426
$N'_{\dot{v}v^2}$	2311	1945	5025	10049
$N'_{\dot{r}}$	−576	−461	−401	−231
$N'_{\dot{r}r^2}$	−130	−250	132	0
N'_0	67	9	0	0
N'_u	−144	37	8	−36
N'_v	−5544	−6570	−3800	−3919
$N'_{|v|}$	−132	0	0	0
N'_{v^3}	−2718	−16602	−23865	−33857
N'_{vu}	0	−1146	−2179	−3666
N'_{vr^2}	3448	4421	−4586	0
$N'_{v\delta^2}$	2317	0	1418	570
N'_r	−3074	−2900	−1960	−2579
N'_{r^2}	0	−45	0	0
N'_{r^3}	−865	−1919	−729	−2253
N'_{ru}	0	0	−473	0
N'_{ru^2}	913	0	0	0
N'_{rv^2}	−16196	−20530	−27858	−60110

Model of	*Tanker*	*Series 60*	*Container*	*Ferry*
$N'_{r\delta^2}$	−324	0	−404	237
N'_{δ}	−1402	−1435	−793	−1621
N'_{δ^2}	0	−138	0	−73
N'_{δ^3}	−1641	3907	0	0
N'_{δ^4}	−536	0	0	0
N'_{δ^5}	2220	−2622	652	2886
$N'_{\delta v^2}$	0	0	−6918	−2950
$N'_{\delta r^2}$	−855	0	−1096	−329
$N'_{\delta u}$	2321	1856	0	2259
$N'_{\delta u^2}$	0	−568	0	0
$N'_{\delta^2 u}$	316	0	0	0
$N'_{\delta^3 u}$	−1538	−1964	0	−1382
$N'_{v|v|}$	0	5328	8103	0
$N'_{r|r|}$	0	0	−1784	0
$N'_{\dot{v}r}$	−394	0	0	0
$N'_{\delta|\delta|}$	384	−1030	0	0
$N'_{\dot{v}^3 u}$	−27133	−13452	0	0
$N'_{r^3 u}$	0	−476	0	−1322

2. For steady turning motion ($\dot{\vec{u}}' = 0$), the original linearized equation of motion simplifies to:

$$D'\vec{u}' = \vec{r}'\delta \tag{6.12}$$

Solving this equation for r' yields:

$$r = \frac{Y'_\delta N_v - Y_v N_\delta}{Y'_v(Y'_r - m')C'}\delta \tag{6.13}$$

C' is the yaw stability index:

$$C' = \frac{N'_r - m'x'_G}{-m'} - \frac{N'_v}{Y'_v} \tag{6.14}$$

$Y'_v(Y'_r - m')$ is positive, the nominator (almost) always negative. Thus C' determines the sign of r'. Positive C' indicates yaw stability, negative C' yaw instability. Yaw instability is the tendency of the ship to increase the absolute value of an existing drift angle. However, the formula is numerically very sensitive and measured coefficients are often too

inaccurate for predictions. Therefore, usually more complicated analyses are necessary to determine yaw stability.

3. If the transverse velocity in the equation of motion is eliminated, we obtain a differential equation of second order of the form:

$$T_1 T_2 \ddot{r} + (T_1 + T_2) \cdot \dot{r} + r = -K(\delta + T_2 \dot{\delta}) \tag{6.15}$$

The T_i are time constants. $|T_2|$ is much smaller than $|T_1|$ and thus may be neglected, especially since linearized equations are anyway a (too) strong simplification of the problem, yielding the simple 'Nomoto' equation:

$$T\dot{r} + r = -K\delta \tag{6.16}$$

T and K here denote time constants. K is sometimes called rudder effectiveness. This simplified equation neglects not only all non-linear effects, but also the influence of transverse speed, longitudinal speed, and heel. As a result, the predictions are too inaccurate for most practical purposes. The Nomoto equation allows, however, a quick estimate of rudder effects on course changes. A slightly better approximation is the 'Norrbin' equation:

$$T\dot{r} + r + \alpha r^3 = -K\delta \tag{6.17}$$

α here is a non-linear 'damping' factor of the turning motions. The constants are determined by matching measured or computed motions to fit the equations best. The Norrbin equation still does not contain any unsymmetrical terms, but for single-screw ships the turning direction of the propeller introduces an asymmetry, making the Norrbin equation questionable.

4. The stability index is difficult to compute due to the numeric sensitivity. Subsequently, the slope of the spiral curve in the origin (for three degrees of freedom) has gained popularity as a single, relatively simple indicator for ships that handle 'correctly':

$$\frac{N'_{v'} \cdot Y'_{\delta} - Y'_{v'} \cdot N'_{\delta}}{Y'_{v'}(N'_{r'} - m'x'_g) - N'_{v'}(Y'_{r'} - m')} < 0 \tag{6.18}$$

The following regression formulae for linear velocity and acceleration coefficients have been proposed (Clarke et al. 1983):

$$Y'_{\dot{v}} = -\pi(T/L)^2 \cdot (1 + 0.16C_B \cdot B/T - 5.1(B/L)^2) \tag{6.19}$$

$$Y'_{\dot{r}} = -\pi(T/L)^2 \cdot (0.67B/L - 0.0033(B/T)^2) \tag{6.20}$$

$$N'_{\dot{v}} = -\pi(T/L)^2 \cdot (1.1B/L - 0.041B/T) \tag{6.21}$$

$$N'_{\dot{r}} = -\pi(T/L)^2 \cdot (1/12 + 0.017C_B \cdot B/T - 0.33B/L) \tag{6.22}$$

$$Y'_v = -\pi(T/L)^2 \cdot (1 + 0.40C_B \cdot B/T) \tag{6.23}$$

$$Y'_r = -\pi(T/L)^2 \cdot (-0.5 + 2.2B/L - 0.08B/T) \tag{6.24}$$

$$N'_v = -\pi(T/L)^2 \cdot (0.5 + 2.4T/L) \tag{6.25}$$

$$N'_r = -\pi(T/L)^2 \cdot (0.25 + 0.039B/T - 0.56B/L) \tag{6.26}$$

T is the mean draft. These formulae apply to ships on even keel. For ships with draft difference $t = T_{ap} - T_{fp}$, correction factors may be applied to the linear even-keel velocity coefficients (Inoue and Kijima 1978):

$$Y'_v(t) = Y'_v(0) \cdot (1 + 0.67t/T) \tag{6.27}$$

$$Y'_r(t) = Y'_r(0) \cdot (1 + 0.80t/T) \tag{6.28}$$

$$N'_v(t) = N'_v(0) \cdot (1 - 0.27t/T \cdot Y'_v(0)/N'_v(0)) \tag{6.29}$$

$$N'_r(t) = N'_r(0) \cdot (1 + 0.30t/T) \tag{6.30}$$

These formulae are based both on theoretical considerations and on model experiments with four 2.5 m models of the Series 60 with different block coefficients for $0.2 < t/T < 0.6$.

In cases where u and/or the propeller turning rate n vary strongly during a maneuver or even change sign as in a stopping maneuver, the above coefficients will vary widely. Therefore, the so-called four-quadrant equations (e.g. Sharma 1986) are better suited to represent the forces. These equations are based on a physical explanation of the forces due to hull, rudder, and propeller, combined with coefficients to be determined in experiments.

6.2.3. Physical Explanation and Force Estimation

In the following, forces due to non-zero rudder angles are not considered. If the rudder at the midship position is treated as part of the ship's body, only the difference between rudder forces at the actual rudder angle δ and those at $\delta = 0°$ have to be added to the body forces treated here. The gap between ship stern and rudder may be disregarded in this case. Propeller forces and hull resistance in straightforward motion are neglected here.

We use a coordinate system with origin fixed at the midship section on the ship's center plane at the height of the center of gravity (Fig. 6.1). The x-axis points forward, y to starboard, z vertically downward. Thus the system participates in the motions u, v, and r of the ship, but does not follow the ship's heeling motion. This simplifies the integration in time (e.g. by

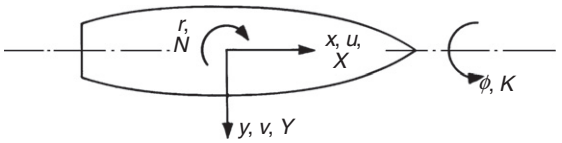

Figure 6.1:
Coordinates *x, y*; direction of velocities *u, v, r*, forces *X, Y*, and moments *K, N*

a Runge−Kutta scheme) of the ship's position from the velocities *u, v, r* and eliminates several terms in the force formulae.

Hydrodynamic body forces can be imagined to result from the change of momentum (= mass · velocity) of the water near to the ship. Most important in maneuvering is the transverse force acting upon the hull per unit length (e.g. meter) in the x-direction. According to the slender-body theory, this force is equal to the time rate of change of the transverse momentum of the water in a 'strip' between two transverse planes spaced one unit length. In such a 'strip' the water near to the ship's side mostly follows the transverse motion of the respective ship section, whereas water farther from the hull is less influenced by transverse ship motions. The total effect of this water motion on the transverse force is the same as if a certain 'added mass' per length m' moved exactly like the ship section in transverse direction. (This approach is thus similar to the strip method approach in ship seakeeping.)

The added mass m' may be determined for any ship section as:

$$m' = \frac{1}{2}\pi \cdot \rho \cdot T_x^2 \cdot c_y \tag{6.31}$$

T_x is the section draft and c_y a coefficient. c_y may be calculated:

- analytically if we approximate the actual ship section by a 'Lewis section' (conformal mapping of a semicircle); Figure 6.2 shows such solutions for parameters (T_x/B) and β = immersed section area/$(B \cdot T_x)$;
- for arbitrary shape by a close-fit boundary element method as for 'strips' in seakeeping strip methods, but for maneuvering the free surface is generally neglected;
- by field methods including viscosity effects.

Neglecting influences due to heel velocity $\dot{\phi}$ and heel acceleration $\ddot{\phi}$, the time rate of change of the transverse momentum of the 'added mass' per length is:

$$\left(\frac{\partial}{\partial t} - u \cdot \frac{\partial}{\partial x}\right)[m'(v + x \cdot r)] \tag{6.32}$$

$\partial/\partial t$ takes account of the local change of momentum (for fixed x) with time t. The term $u \cdot \partial/\partial x$ results from the convective change of momentum due to the longitudinal motion of the water 'strip' along the hull with appropriate velocity $-u$ (i.e. from bow to stern). $v + x \cdot r$ is the

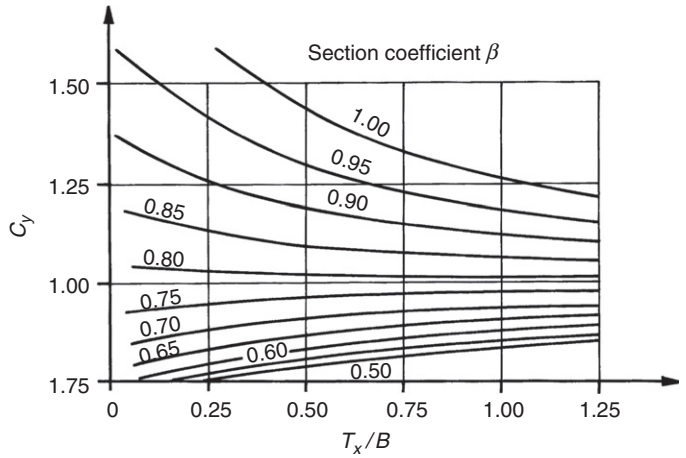

Figure 6.2:
Section added mass coefficient c_y for low-frequency, low-speed horizontal acceleration

transverse velocity of the section in the *y*-direction resulting from both transverse speed *v* at midship section and the yaw rate *r*. The total transverse force is obtained by integrating the above expression over the underwater ship length *L*. The yaw moment is obtained by multiplying each force element with the respective lever *x*, and the heel moment is obtained by using the vertical moment $z_y m'$ instead of m', where z_y is the depth coordinate of the center of gravity of the added mass. For Lewis sections, this quantity can be calculated theoretically (Fig. 6.3). For CFD approaches the corresponding vertical moment is computed directly as part

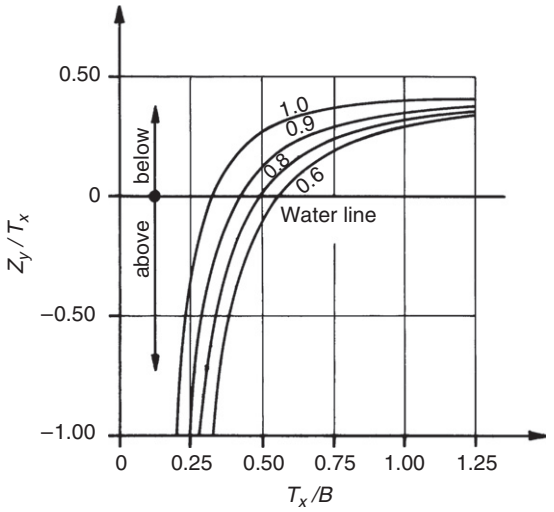

Figure 6.3:
Height coordinate z_y of section added mass m'

of the numerical solution. Söding gives a short FORTRAN subroutine to determine c_y and z_y for Lewis sections in Brix (1993, p. 252).

Based on these considerations we obtain the 'slender-body contribution' to the forces as:

$$\begin{Bmatrix} X \\ Y \\ K \\ N \end{Bmatrix} = \int_L \begin{Bmatrix} 0 \\ 1 \\ 1 \\ x \end{Bmatrix} \cdot \left(\frac{\partial}{\partial t} - u \cdot \frac{\partial}{\partial x} \right) \left(m'(v + x \cdot r) \right) \cdot \left(\begin{Bmatrix} 0 \\ m' \\ -z_y m' \\ m' \end{Bmatrix} (v + x \cdot r) \right) \mathrm{d}x \quad (6.33)$$

The 'slender-body contribution' to X is zero. Several modifications to this basic formula are necessary or at least advisable:

1. For terms involving $-\partial/\partial t$, i.e. for the acceleration-dependent parts of the forces, correction factors k_1, k_2 should be applied. They consider the lengthwise flow of water around bow and stern which is initially disregarded in determining the sectional added mass m'. The acceleration part of the above basic formula then becomes:

$$\begin{Bmatrix} X_1 \\ Y_1 \\ K_1 \\ N_1 \end{Bmatrix} = \int_L \begin{Bmatrix} 0 \\ -k_1 m' \\ z_y m' \\ -k_2 x m' \end{Bmatrix} \cdot (k_1 \dot{v} + k_2 x \cdot \dot{r}) \, \mathrm{d}x \quad (6.34)$$

   k_1 and k_2 are approximated here by regression formulae which were derived from the results of three-dimensional flow calculations for accelerated ellipsoids:

$$k_1 = \sqrt{1 - 0.245\varepsilon - 1.68\varepsilon^2} \quad (6.35)$$

$$k_2 = \sqrt{1 - 0.76\varepsilon - 4.41\varepsilon^2} \quad (6.36)$$

   with $\varepsilon = 2T_x/L$.

2. For parts in the basic formula due to $u \cdot \partial/\partial x$, one should distinguish terms where $\partial/\partial x$ is applied to the first factor containing m' from terms where the second factor $v + x \cdot r$ is differentiated with respect to x (which results in r). For the former terms, it was found by comparison with experimental values that the integral should be extended only over the region where $\mathrm{d}m'/\mathrm{d}x$ is negative, i.e. over the forebody. This may be understood as the effect of flow separation in the aftbody. The flow separation causes the water to retain most of its transverse momentum behind the position of maximum added mass, which for ships without trim may be taken to be the midship section. The latter terms, however, should be integrated over the full length of the ship. This results in:

$$\begin{Bmatrix} X_2 \\ Y_2 \\ K_2 \\ N_2 \end{Bmatrix} = u \begin{Bmatrix} 0 \\ -m'_m \\ z_{ym} m'_m \\ -x_m m'_m \end{Bmatrix} \cdot (v + x_m \cdot r) + u \cdot r \int_{x_a}^{x_m} \begin{Bmatrix} 0 \\ m' \\ -z_{ym} m' \\ x m' \end{Bmatrix} \mathrm{d}x - u \int_{x_m}^{x_f} \begin{Bmatrix} 0 \\ 0 \\ 0 \\ m' \end{Bmatrix} (v + x \cdot r)\, \mathrm{d}x \tag{6.37}$$

x_a is the x coordinate of the aft end, x_f of the forward end of the ship. The index m refers to the x coordinate where m' is maximum. For negative u the differences in treating the fore- and aftbody are interchanged.

3. The slender-body theory disregards longitudinal forces associated with the added mass of the ship in the longitudinal direction. These additional terms are taken from potential-flow theory without flow separation (Newman 1977):

$$\begin{Bmatrix} X_3 \\ Y_3 \\ K_3 \\ N_3 \end{Bmatrix} = \begin{Bmatrix} -m_x \cdot \dot{u} \\ -m_x \cdot u \cdot r \\ 0 \\ -m_x \cdot u \cdot v \end{Bmatrix} \tag{6.38}$$

m_x is the added mass for longitudinal motion; it may be approximated by a formula which was also fitted to theoretical values for ellipsoids:

$$m_x = \frac{m}{\pi \sqrt{L^3/\nabla} - 14} \tag{6.39}$$

∇ denotes here the volume displacement. Theoretically additional terms proportional to $r \cdot v$ and r^2 should appear in the formula for X. According to experiments with ship models, however, the $r \cdot v$ term is much smaller and the r^2 term may even have a different sign than the theoretical expression. Therefore these terms, which are influenced substantially by flow separation, have been omitted. Further, some theoretical terms of small magnitude involving heeling motion or referring to the heeling moment have also been omitted in the above formula for X_3, etc.

4. Because slender-body theory neglects flow separation in transverse flow around ship sections (only longitudinal flow separation is roughly taken into account), an additional 'cross-flow resistance' of the ship sections has to be added. The absolute value of this resistance per unit length is:

$$\frac{1}{2} \rho \cdot T_x \cdot v_x^2 \cdot C_D \tag{6.40}$$

$v_x = v + x \cdot r$ is the transverse velocity of the section. C_D is a cross-flow resistance coefficient. The direction of the resistance is opposite to the direction of v_x. Thus for

arbitrary direction of motion, the term $-v_x|v_x|$ is required instead of v_x^2. Therefore the cross-flow resistance adds the following contributions to the body forces:

$$\begin{Bmatrix} X_4 \\ Y_4 \\ K_4 \\ N_4 \end{Bmatrix} = \frac{1}{2}\rho \int_L \begin{Bmatrix} 0 \\ -1 \\ z_D \\ -x \end{Bmatrix} (v + x \cdot r) \cdot |v + x \cdot r| \cdot T_x C_D \, \mathrm{d}x \tag{6.41}$$

z_D is the z coordinate (measured downward from the center of gravity G of ship's mass m) of the action line of the cross-flow resistance. For typical cargo ship hull forms, this force acts on about 65% of the draft above the keel line. Thus a constant (mean) value over ship length of:

$$z_D = \overline{KG} - 0.65T \tag{6.42}$$

may be applied to the formula for X_4, etc. For tug models, values of 1.0 ± 0.1 instead of the above 0.65 were found.

C_D is estimated as 1.0 averaged over the whole ship length for cargo vessels like container ships with bilge keels. For fuller hulls values between 0.5 and 0.7 may be suitable. The C_D values are generally higher in the aftbody than in the forebody due to stronger flow separation in the aftbody.

Results of transverse towing tests (at zero speed) with and without heel with large models are presented in Table 6.3. These results differ from the situation at considerable forward speed.

The sum of contributions 1 to 4 constitutes the total body force:

$$\begin{Bmatrix} X \\ Y \\ K \\ N \end{Bmatrix} = \begin{Bmatrix} X_1 \\ Y_1 \\ K_1 \\ N_1 \end{Bmatrix} + \begin{Bmatrix} X_2 \\ Y_2 \\ K_2 \\ N_2 \end{Bmatrix} + \begin{Bmatrix} X_3 \\ Y_3 \\ K_3 \\ N_3 \end{Bmatrix} + \begin{Bmatrix} X_4 \\ Y_4 \\ K_4 \\ N_4 \end{Bmatrix} \tag{6.43}$$

Table 6.3: Results of transverse towing tests with large models upright and with 10° heel; models were equipped with rudder and propeller but without bilge keels

	Cargo ship	Tanker	Tanker	Container ship	Twin-screw salvage tug
L/B	6.66	5.83	6.11	7.61	5.21
B/T	2.46	2.43	2.96	2.93	2.25
C_B	0.66	0.84	0.81	0.58	0.58
C_D	0.562	0.983	0.594	0.791	0.826
$C_{D10°}$	0.511	1.151	–	1.014	–

For steady traversing or pure yaw motion without forward speed, only terms listed under 4 above are relevant.

The yaw stability is very sensitive to small changes in the body forces. Therefore a reliable prediction of yaw stability based on the slender-body theory or regression analysis of model tests is not possible. Substantial improvements of theoretical calculations seem possible only if the flow separation around the hull is determined in detail by computational simulation of the viscous, turbulent flow in a RANSE code (with appropriate turbulence model) or even LES simulations. However, the slender-body approach described here appears to be useful and sufficient in most cases in deep water. Extensions of the theory to shallow water exist.

6.2.4. Influence of Heel

For exact motion predictions including the coupling of maneuvering motions with heel one should take account of:

- the heeling moments due to weight and mass moments, hydrostatic and hydrodynamic moments on hull, rudder, and propeller, and possibly wind heeling moments or other external influences;
- the dependence of *X, Y,* and *N* on heel angle, heel velocity, and heel acceleration.

Details may be drawn from Bohlmann's (1989, 1990) work on submarine maneuvering.

By choosing our coordinate origin at the height of the ship's center of gravity, many of these influences are zero, others are small in cargo ships. For example, the dependence of *X, Y,* and *N* on the heel rate and heel acceleration can be neglected if the interest is not in the rolling motions themselves, but only in their influence on maneuvering motions. In this case, the heel angle may be determined by the equilibrium resulting from the maneuvering heel moment *K* as stated before, the hydrostatic righting moment, and possibly the wind- and propeller-induced moments. However, the dependence of *X, Y,* and *N* on the heel angle may be substantial.

The following procedure is recommended to evaluate the influence of heel:

1. In the equations for X_1 etc., m' is determined taking into account the heel angle. This leads to larger m' values in the midship range due to increase of draft with heel for the full midship sections. Capturing the influence of heel in the computations of m' is straightforward in CFD computations, but also a Lewis transformation approach can be extended to include heel (Söding 1984).
2. In the equations for X_1, instead of v the expression $v - u \cdot \partial y_B/\partial x$ should be used, where y_B is the y coordinate of the center of gravity of the immersed section area due to heel. The term takes account of the curvature of the 'centerline' of the heeled hull.
3. The cross-flow resistance coefficient C_D depends on the heel angle. C_D may decrease by 1−3% per degree of heel in the direction of drift motion. Due to the increase of section

draft (at least in the midship region) with heel, however, the actual cross-flow resistance may increase with heel angle.

4. For larger heel angles exceeding approximately 25°, the cross-flow velocity in the equation for X_4, etc. should be determined with respect to the curved line being composed of the points of maximum draft of the ship sections. If this line has transverse coordinate $y_T(x)$, instead of $v + x \cdot r$ the expression $v + x \cdot r - \partial y_T/\partial x \cdot u$ has to be used in the equation for X_4, etc. for heel angles exceeding 25°. For smaller heel, a linear interpolation of the correction term $\partial y_T/\partial x \cdot u$ over heel is recommended.

This procedure improves predictions, but still has substantial deficiencies for larger heel angles.

6.2.5. Shallow Water and Other Influences

Body forces depend not only on the actual acceleration, speed, and (in case of heel) state of the vessel, but also on the previous time history of body motion. This is due to vortex shedding and waves generated by the ship. However, these 'memory effects' are very small in ordinary maneuvering motions. Exceptions where memory effects may be important are:

- PMM experiments with the usual too small amplitudes;
- self-induced motions of a moored ship.

Shallow water, non-uniform current and interactions with other ships may substantially influence the body forces as discussed in detail in Brix (1993). The influence of shallow water can be roughly described as follows. If the ship keel is just touching the sea bottom, the effective side ratio of the ship hull is increased from approximately 0.1 (namely $2T/L$; factor 2 due to mirror image at waterplane) to ∞. This increases the transverse forces by approximately a factor of 40 (following the simple estimate formula for rudder lift in Section 6.4). The rudder itself increases its effective side ratio from approximately 2 for deep water to ∞ for extremely shallow water. The rudder forces are then increased by a factor of approximately 2.6. The hull forces for a yaw stable ship decrease the course-changing ability, the rudder forces increase the course-changing ability. Since the hull forces increase more than the rudder forces on shallow water, the net result for yaw stable ships is:

- increased radius of turning circle;
- increased turning time;
- increased yaw checking time.

For yaw instable ships, this may be different, especially if the yaw stability changes drastically. Shallow water may increase or decrease yaw stability. One of several effects is the change of trim. Boundary element methods, namely 'wave resistance' codes, may be used to predict trim and sinkage of real ship geometries, usually with good accuracy on shallow water. The results of such computations have been used to estimate the amount of yaw instability.

6.2.6. Stopping

The rudder behind a reverse turning propeller is almost without effect. The track of a stopping ship is thus largely determined by the maneuvering forces of the propeller(s) and wind. For yaw instable ships, the track can be largely influenced by small initial port or starboard motions. For sister ships (large tankers) under 'same' conditions, stopping times vary between 12 and 22 minutes with largely differing tracks. The differences are attributed to such small (random) initial differences in yaw motions.

For low speeds, the stopping times and distances can be determined as follows. One assumes that between two points in time t_1 and t_2 the reverse thrust (minus thrust deduction) T is approximately constant and that the resistance R is proportional to speed u:

$$\frac{R}{u^2} = \frac{R_0}{U_0^2} = k \tag{6.44}$$

k is the stopping constant. The index 0 denotes the values at the beginning of the maneuver. If we assume a straight stopping track, the fundamental equation of motion is:

$$m \cdot \dot{u} = -k(u^2 + u_T^2) \tag{6.45}$$

The mass m includes the hydrodynamic added mass m'' for longitudinal motion which may be estimated by Eq. (6.39). $u_T = U_0\sqrt{T/R_0}$ is the speed the ship would have after a long time if the thrust T were directed forward. The above differential equation can be solved (by separation of variables) to yield:

$$\Delta t = t_2 - t_1 = \frac{m}{k u_T}\left[\arctan\frac{u_1}{u_T} - \arctan\frac{u_2}{u_T}\right] \tag{6.46}$$

The distance is given by multiplying the above differential equation by $u = \mathrm{d}s/\mathrm{d}t$ and solving again (by separation of variables) to yield:

$$\Delta s = s_2 - s_1 = \frac{m}{2k}\ln\left(\frac{u_1^2 + u_T^2}{u_2^2 + u_T^2}\right) \tag{6.47}$$

These two equations for Δt and Δs can be used to compute stepwise the stopping process by splitting the process into time intervals where the thrust T can be assumed to be constant. The reverse thrust is best determined by using four-quadrant diagrams for the propellers, if these diagrams are available.

6.2.7. Jet Thrusters

Transverse jet thrusters consist of a transverse pipe through the ship hull usually located at the bow or at the stern. The pipe contains a screw propeller which pumps water either to port or

starboard, thus creating a side thrust (and moment). The purpose of a jet thruster is to increase maneuverability at low speeds, allowing the ship to maneuver with no or less tug assistance. As the rudder astern already supplies maneuvering forces, jet thrusters are more effective at the bow and usually placed there ('bow thrusters'). Also, stern jets need to cope with potential collision problems in arranging both jet pipe and propeller shaft. Jet thrusters may also serve as an emergency backup for the main rudder. Backups for rudders are needed for ships with dangerous cargo. Jet thrusters are less attractive for ships on long-distance routes calling at few ports. The savings in tug fees may be less than the additional expense for fuel.

For ocean-going ships, side thrusts of 0.08−0.12 kN per square meter underwater lateral area are typical values. These values relate to zero forward speed of the ship. Installed power P, cross-section area of the pipe A, and flow velocity v in the jet thruster are related by:

$$T = \rho \cdot A \cdot v^2 \tag{6.48}$$

$$P = \frac{1}{\eta} \cdot \frac{1}{2} \rho \cdot A \cdot v^3 \tag{6.49}$$

η is here the efficiency of the thruster propeller. These equations yield:

$$\frac{P}{T} = \frac{v}{2\eta} \tag{6.50}$$

$$\frac{T}{A} = \rho v^2 \tag{6.51}$$

$\eta = 0.8$ and $v = 11$ m/s yield typical relations: approximately 120 kN/m^2 thrust per thruster cross-section area and 7 kW power per kN thrust.

With increasing speed, jet thrusters become less effective and rudders become more effective. The reason is that the jet is bent backwards and may reattach to the ship hull. The thrust is then partially compensated by an opposite suction force. This effect may be reduced by installing a second (passive) pipe without a propeller downstream of the thruster (Brix 1993).

6.2.8. CFD for Ship Maneuvering

For most ships, the linear system of equations determining the drift and yaw velocity in steady turning motion is nearly singular. This produces large relative errors in the predicted steady turning rate, especially for small rudder angles and turning rates. For large rudder angle and turning rate, non-linear forces alleviate these problems somewhat. But non-linear hull forces depend crucially on the cross-flow resistance or the direction of the longitudinal vortices, i.e. on quantities which are determined empirically and which vary widely. In addition, extreme rudder forces depend strongly on the rudder stall angle which − for a rudder behind the hull and propeller − requires at least two-dimensional RANSE simulations. Thus large errors are

frequently made in predicting both the ship's path in hard maneuvers and the course-keeping qualities. (The prediction of the full ship is fortunately easier as at the higher Reynolds numbers stall rarely occurs.) In spite of that, published comparisons between predictions and measurements based on inviscid, classical approaches have indicated almost always excellent accuracy; a notable exception is Söding (1993). The difference is that Söding avoids all information which would not be available had the respective model not been tested previously. The typical very good agreement published by others is then suspected to be either chosen as best results from a larger set of predictions or due to empirical corrections of the calculation method based on experiments which include the ship used for demonstrating the attained accuracy. Naturally, these tricks are not possible for a practical prediction where no previous test results for the ship design can be used. Thus accurate maneuvering predictions require RANSE approaches, and even then care has to be taken in grid generation and turbulence modeling. It may also be possible to predict full-scale ship motions with sufficient accuracy, but the experience published so far is insufficient to establish this as state of the art. However, differences between alternative designs and totally unacceptable designs may be detected using simper methods for maneuvering prediction.

The simplest approach to body force computations is the use of regression formulae based on slender-body theory, but with empirical coefficients found from analyzing various model experiments, e.g. Clarke et al. (1983). The next more sophisticated approach would be to apply slender-body methods directly, deriving the added mass terms for each strip from analytical (Lewis form) or BEM computations. The application of three-dimensional RANSE methods yields the best results, but only a few industry applications had appeared by 2010. The main individual approaches are ranked in increasing complexity:

- *Lifting surface methods*
  An alternative to slender-body theory, applicable to rudder and hull (separately or in combination), is the lifting surface model. It models the inviscid flow about a plate (center plane), satisfying the Kutta condition (smooth flow at the trailing edge) and usually the free-surface condition for zero F_n (double-body flow). The flow is determined as a superposition of horseshoe vortices which are symmetrical with respect to the water surface (mirror plane). The strength of each horseshoe vortex is determined by a collocation method from Biot–Savart's law. For stationary flow conditions, in the ship's wake there are no vertical vortex lines, whereas in instationary flow vertical vortex lines are required also in the wake. The vortex strength in the wake follows from three conditions:
  1. Vortex lines in the wake flow backwards with the surrounding fluid velocity, approximately with the ship speed u.
  2. If the sum of vertical ('bound') vortex strength increases over time within the body (due to larger angles of attack), a corresponding negative vorticity leaves the trailing edge, entering into the wake.
  3. The vertical vortex density is continuous at the trailing edge.

Except for a ship in waves, it seems accurate enough to use the stationary vortex model for maneuvering investigations.

Vortex strengths within the body are determined from the condition that the flow is parallel to the midship (or rudder) plane at a number of collocation points. The vortices are located at one-quarter of the chord length from the bow, the collocation points at three-quarters of the chord length from the bow. This gives a system of linear equations to determine the vortex strengths. Transverse forces on the body may then be determined from the law of Kutta–Joukowski, i.e. the body force is the force exerted on all 'bound' (vertical) vortices by the surrounding flow.

Alternatively, one can smooth the bound vorticity over the plate length, determine the pressure difference between port and starboard of the plate, and integrate this pressure difference. For shallow water, reflections of the vortices are necessary both at the water surface and at the bottom. This produces an infinite number of reflections, a subset of which is used in numerical approximations. If the horizontal vortex lines are arranged in the ship's center plane, only transverse forces depending linearly on v and r are generated. The equivalent to the non-linear cross-flow forces in slender-body theory is found in the vortex models if the horizontal vortex lines are oblique to the center plane. Theoretically the position of the vortex lines could be determined iteratively to ensure that they move with the surrounding fluid flow which is influenced by all other vortices. But practically this procedure is usually not applied because of the high computing effort and convergence problems. According to classical foil theory, the direction of the horizontal vortices should be halfway between the ship longitudinal direction and the motion direction in deep water. More modern procedures arrange the vortices in the longitudinal direction within the ship length, but in an oblique plane (for steady motion at a constant yaw angle) or on a circular cylinder (for steady turning motion) in the wake. The exact direction of the vortices is determined depending on water depth. Also important is the arrangement of vortex lines and collocation points on the material plate. Collocation points should be about halfway between vortex lines in both longitudinal and vertical directions. High accuracy with few vortex lines is attained if the distance between vertical vortices is smaller at both ends of the body, and if the distance between horizontal vortices is small at the keel and large at the waterline.

- *Lifting body methods*

  A body with finite thickness generates larger lift forces than a plate. This can be taken into account in different ways:

  1. by arranging horseshoe vortices (or dipoles) on the hull on both sides;
  2. by arranging a source and a vortex distribution on the center plane;
  3. by arranging source distributions on the hull and a vortex distribution on the center plane.

  In the third case, the longitudinal distribution of bound vorticity can be prescribed arbitrarily, whereas the vertical distribution has to be determined from the Kutta condition along the

trailing edge. The Kutta condition can be approximated in different ways. One suitable formulation is: the pressure (determined from the Bernoulli equation) should be equal at port and starboard along the trailing edge. If the ship has no sharp edge at the stern (e.g. below the propeller's axis for a stern bulb), it is not clear where the flow separation (and thus the Kutta condition) should be assumed. This may cause large errors for transverse forces for the hull alone, but when the rudder is modeled together with the hull, the uncertainty is much smaller. Forces can be determined by integrating the pressure over the hull surface. For a very thin body, the lifting surface and lifting body models should result in similar forces. In practice, however, large differences are found. The lifting-body model with source distributions on both sides of the body has difficulties if the body has a sharp bow. Assuming a small radius at the bow waterline produces much better results. For a ship hull it seems difficult to obtain more accurate results from lifting-body theory than using slender-body theory. For the rudder and for the interaction between rudder and hull, however, lifting-surface or lifting-body theory is the method of choice for angles of attack where no stall is expected to occur. Beyond the stall angle, only RANSE methods (or even more sophisticated viscous flow computations) may be used.

By the early 1990s research applications for lifting-body computations including free-surface effects appeared for steady drift motions. The approach of Zou (1990) is typical. First the wave resistance problem is solved including dynamic trim and sinkage. Assuming small asymmetry, the difference between symmetrical and asymmetrical flow is linearized. The asymmetrical flow is then determined by a lifting-body method with an additional source distribution above the free surface.

- *Field methods*

  In spite of the importance of viscosity for maneuvering, viscous hull force calculations appeared in the 1990s only as research applications and were mostly limited to steady flow computations around a ship with a constant yaw angle. By 2010, simulations for freely maneuvering ships, even in waves, were presented in research applications. However, industry applications still relied largely on inviscid approaches with semi-empirical corrections, due to the large required resources for RANSE maneuvering simulations. Difficulties in RANSE computations for maneuvering are:

  - The number of computational cells is much higher than for resistance computations, because both port and starboard sides must be discretized and because vortices are shed over nearly the full ship length.
  - The large-scale flow separation requires advanced turbulence models, adding to the computational effort.

  State-of-the-art computations for ship hulls at model scale Reynolds numbers were capable of predicting transverse forces and moments well, even for large yaw angles, but predicted the longitudinal force (resistance) with large relative errors. Computations have included dynamic trim and sinkage, which play an important role in shallow-water maneuvering.

RANSE computations including free-surface effects will grow in importance and have started to drift into practical applications. They are expected to substantially improve the accuracy of maneuvering force predictions over the next decade.

6.3. Experimental Approaches

6.3.1. Maneuvering Tests for Full-Scale Ships in Sea Trials

The main maneuvering characteristics as listed in the introduction to maneuvering are quantified in sea trials with the full-scale ship. Usually the design speed is chosen as initial speed in the maneuver. Trial conditions should feature deep water (water depth $>$ 2.5 ship draft), little wind (less than Beaufort 4) and 'calm' water to ensure comparability to other ships. Trim influences the initial turning ability and yaw stability more than draft. For comparison with other ships, the results are made non-dimensional with ship length and ship length travel time (L/V).

The main maneuvers used in sea trials follow recommendations of the Manoeuvring Trial Code of ITTC (1975) and the IMO circular MSC 389 (1985). IMO also specifies the display of some of the results in bridge posters and a maneuvering booklet on board ships in the IMO resolution A.601(15) (1987) (Provision and display of maneuvering information on board ships).

The main maneuvers in sea trials are:

1. *Turning circle test*
   Starting from straight motion at constant speed, the rudder is turned at maximum speed to an angle υ (usually maximum rudder angle) and kept at this angle, until the ship has performed a turning circle of at least 540°. The trial is performed for both port and starboard sides. The essential information obtained from this maneuver (usually by GPS) consists of (Fig. 6.4):
   - tactical diameter;
   - maximum advance;
   - transfer at 90° change of heading;
   - times to change heading 90° and 180°;
   - transfer loss of steady speed.

   Typical values are tactical diameter of 4.5−7L for slender, 2.4−4 L for short and full ships. Decisive is the slenderness ratio $L/\sqrt[3]{\nabla}$, where ∇ is the volume displacement.

   Fast displacement ships with $F_n > 0.25$ may feature dangerously large heel angles in turning circles. The heel is always outwards, i.e. away from the center of the turning circle. (Submarines and boats with dynamic lift like hydrofoils are exceptional in that they may heel inwards.) The heel is induced by the centrifugal force $m \cdot u \cdot r$ acting outwards on the ship's center of gravity, the hull force $Y_v v + Y_r r$ acting inwards, and the much smaller

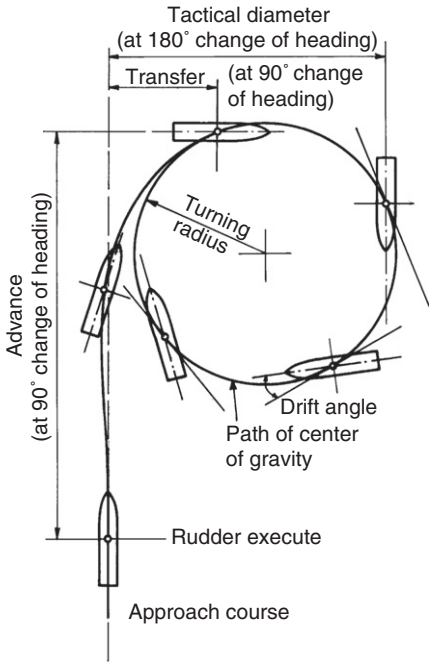

Figure 6.4:
Definitions used on turning circle

rudder force $Y_\delta\delta$ acting outwards. For maneuvering predictions it is important to consider that the ship is faster at the beginning of the turning circle and slower at sustained turning. The heeling angle exceeds dynamically the static heel angle due to forces listed above.

The turning circle test is used to evaluate the turning ability of the ship.

2. *Spiral maneuvers*
   We distinguish between:
   - *'Direct' spiral maneuver (Dieudonne)* – With the ship on an initial straight course, the rudder is put hard to one side until the ship has reached a constant rate of change of heading. The rudder angle is then decreased in steps (typically 5°, but preferably less near zero rudder angle) and again held until a steady condition is reached. This process is repeated until the rudder has covered the whole range to the maximum rudder angle on the other side. The rate of turn is noted for each rudder angle. The test should be performed at least for yaw unstable ships going both from port to starboard and from starboard to port.
   - *'Indirect' (reverse) spiral maneuver (Bech)* – The ship is steered at a constant rate of turn and the mean rudder angle required to produce this yaw rate is measured. This way, points on the curve rate of turn vs. rudder angle may be taken in any order.

   The spiral test results in a curve as shown in Fig. 6.5. The spiral test is used to evaluate the turning ability and the yaw stability of the ship. For yaw unstable ships, there may be three

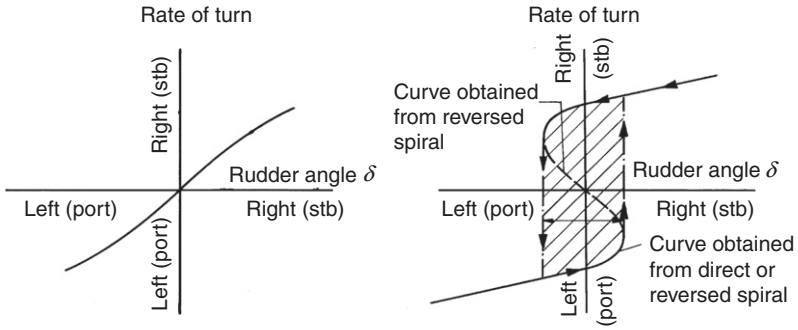

Figure 6.5:
Results of spiral tests for yaw stable and yaw unstable ship

possible rates of turn for one given rudder angle as shown in Fig. 6.5. The one in the middle (dotted line) represents an instable state which can only be found by the indirect method. In the direct method, the rate of turn 'switches' at the vertical sections of the curve suddenly to the other part of the curve if the rudder angle is changed. This is indicated by the dotted arrows in Fig. 6.5.

The spiral test, especially with the direct method, is time-consuming and sensitive to external influences. The results show that a linearization of the body force equations is acceptable only for small $|r|$ (Fig. 6.5). For yaw stable ships, the bandwidth of acceptable rudder angles to give small $|r|$ is small, e.g. $\pm 5°$. For yaw unstable ships, large $|r|$ may result for any δ.

3. *Pull-out maneuver*
After a turning circle with steady rate of turn the rudder is returned to midship. If the ship is yaw stable, the rate of turn will decay to zero for turns both port and starboard. If the ship is yaw unstable, the rate of turn will reduce to some residual rate of turn (Fig. 6.6).

The pull-out maneuver is a simple test to give a quick indication of a ship's yaw stability, but requires very calm weather. If the yaw rate in a pull-out maneuver tends towards a finite value

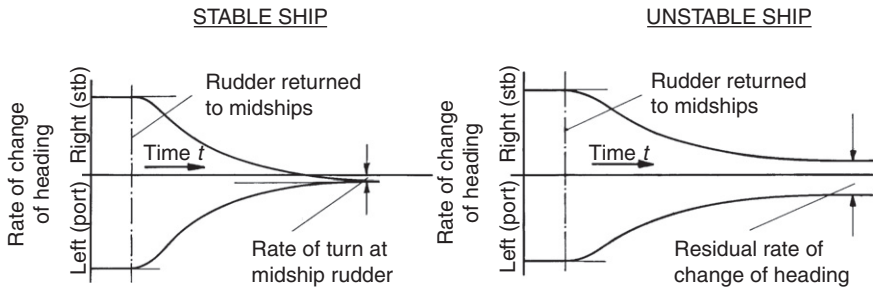

Figure 6.6:
Results of pull-out maneuver

in single-screw ships, this is often interpreted as yaw instability, but it may be at least partially due to the influence of asymmetry induced by the propeller in single-screw ships or wind.

4. *Zigzag maneuver*
   The rudder is reversed alternately by a rudder angle δ to either side at a deviation ψ_e from the initial course. After a steady approach the rudder is put over to starboard (first execute). When the heading is ψ_e off the initial course, the rudder is reversed to the same rudder angle to port at maximum rudder speed (second execute). After counter rudder has been applied, the ship continues turning in the original direction (overshoot) with decreasing turning speed until the yaw motion changes direction. In response to the rudder the ship turns to port. When the heading is ψ_e off the initial course to port, the rudder is reversed again at maximum rudder speed to starboard (third execute). This process continues until a total of, say, five rudder executes have been completed. Typical values for ψ_e are 10° and 20°. The test was especially developed for towing tank tests, but it is also popular for sea trials. The test yields initial turning time, yaw checking time, and overshoot angle (Fig. 6.7).

   For the determination of body force coefficients a modification of the zigzag maneuver is better suited: the incremental zigzag test. Here, after each period other angles δ and ψ_e are chosen to cover the whole range of rudder angles. If the incremental zigzag test is properly executed it may substitute for all other tests as the measured coefficients should be sufficient for an appropriate computer simulation of all other required maneuvering quantities. Figure 6.8 shows results of many model zigzag tests as given by Brix (1993). These yield the following typical values:
   - initial turning time t_a: 1−1.5 ship length travel time;
   - time to check starboard yaw t_s: 0.5−2 ship travel length time (more for fast ships);
   - starboard overshoot angle α_s: 5−15°;
   - turning speed to port r (yaw rate): 0.2−0.4 per ship travel length time.

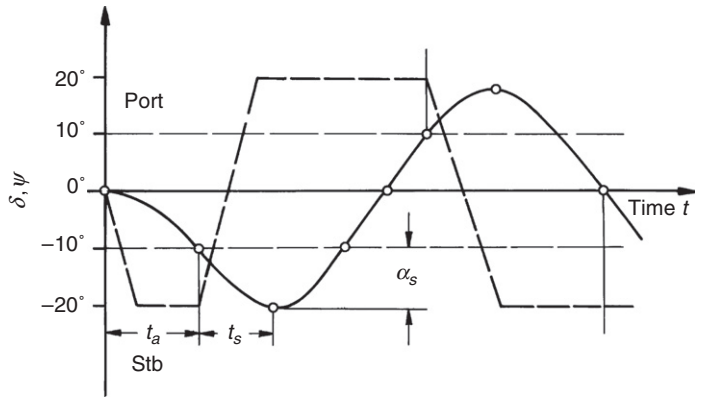

Figure 6.7:
Scheme of zigzag maneuver; t_a initial turning time, t_s yaw checking time, α_s overshoot angle; — — — — rudder angle δ, ——— course angle ψ

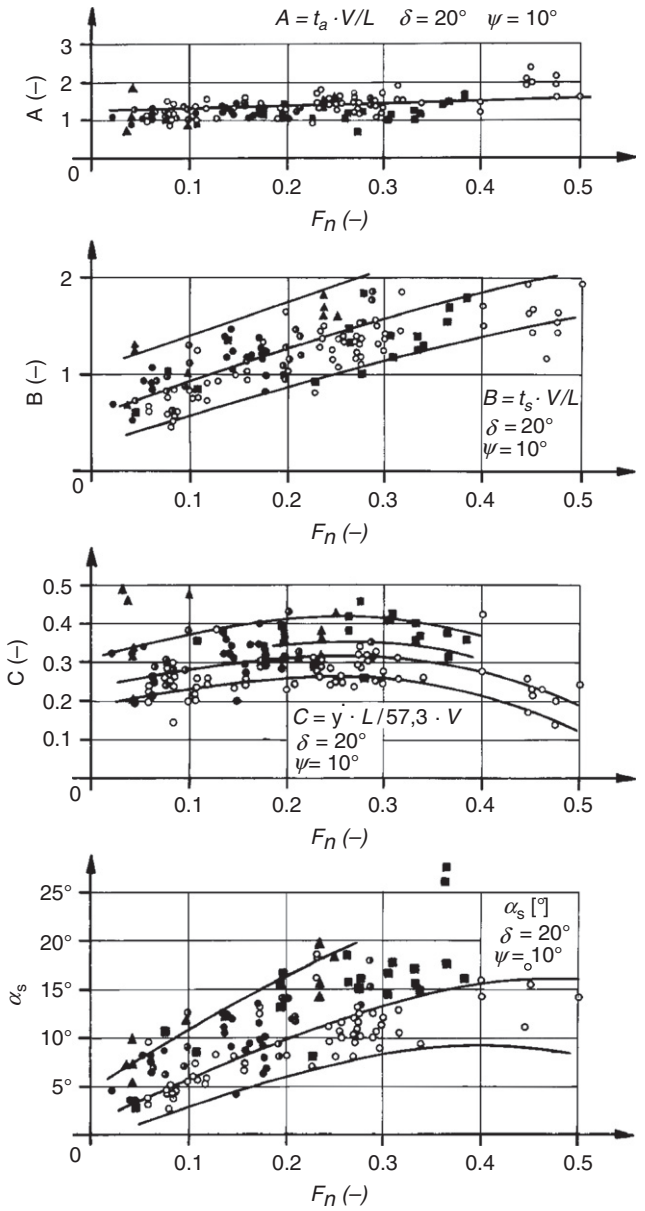

Figure 6.8:
Non-dimensional data obtained from zigzag model tests (Brix 1993); A = non-dimensional initial turning times; $\beta = B$ = non-dimensional times to check starboard yaw; C = non-dimensional turning speed to port; α_s starboard overshoot angle

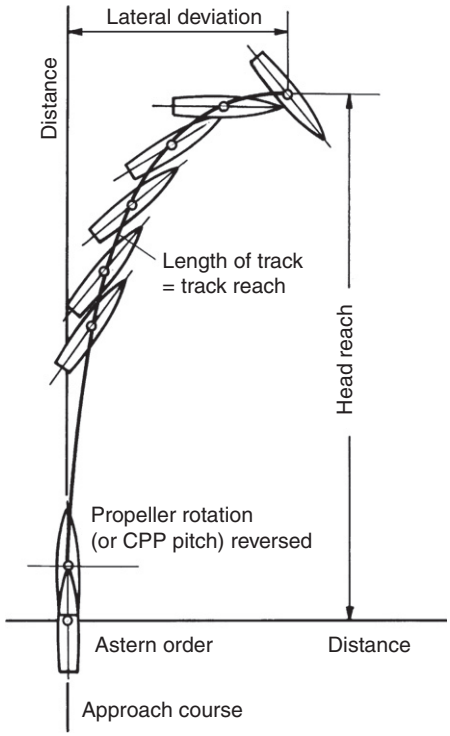

Figure 6.9:
Results of stopping trial

5. *Stopping trial*
   The most common maneuver in stopping trials is the crash-stop from full-ahead speed. For ships equipped with fixed-pitch propellers, the engine is stopped and then as soon as possible reversed at full astern. Controllable-pitch propellers (CPP) allow a direct reversion of the propeller pitch. Sometimes the rudder is kept a midships, sometimes one tries to keep the ship on a straight course, which is difficult as the rudder effectiveness usually decreases drastically during the stopping maneuver and because the reversing propeller induces substantial transverse forces on the aftbody. The reaction to stopping maneuvers is strongly non-linear. Thus environmental influences (e.g. wind) and slight changes in the initial conditions (e.g. slight deviation of the heading to either port or starboard) may change the resulting stopping track considerably.

   The maneuver ends when $u = 0$. Results of the stopping maneuver are (Fig. 6.9):
   - head reach (distance traveled in the direction of the ship's initial course);
   - lateral deviation (distance to port or starboard measured normal to the ship's initial course);
   - stopping time.

Crash-stops from full speed are nautically not sensible as turning usually offers better avoidance strategies involving shorter distances. Therefore stopping maneuvers are also recommended at low speed, because then the maneuver is of practical interest for navigation purposes.

Single-screw ships with propellers turning right (seen from abaft clockwise) will turn to starboard in a stopping maneuver. For controllable-pitch propellers, the propeller pitch is reversed for stopping. Since according to international nautical conventions, collision avoidance maneuvers should be executed with starboard evasion, single-screw ships should be equipped with right-turning fixed-pitch propellers or left-turning CPPs. Simulations of stopping maneuvers typically use the four-quadrant diagrams for propellers to determine the propeller thrust also in astern operation (see Section 2.2, Chapter 2).

6. *Hard rudder test*
With the ship on an initially straight course, the rudder is put hard to 35° port. As soon as this rudder angle is reached (i.e. without waiting for a specific heading or rate of turning), the rudder is reversed to hard starboard. The time for changing the rudder angle from 35° on one side to 30° on the other side must not exceed 28 seconds according to IMO regulations (SOLAS 1960). This regulation is rightfully criticized as the time limit is independent of ship size. The IMO regulation is intended to avoid under-dimensioning of the rudder gear.
7. *Man-overboard maneuver (Williamson turn)*
This maneuver brings the ship in minimum time on opposite heading and same track as at the beginning of the maneuver, e.g. to search for a man overboard. The rudder is laid initially hard starboard, at, say, 60° (relative to the initial heading) hard port, and at, say, −130° to midship position again (Fig. 6.10). The appropriate angles (60°, −130°) vary with each ship and loading condition and have to be determined individually such that at the end of the maneuver the deviation in heading is approximately 180° and in track approximately zero. This is determined in trial-and-error tests during ship trials. However, an approximate starting point is determined in computational simulations beforehand.

6.3.2. Model Tests

Model tests to evaluate maneuverability are usually performed with models ranging between 2.5 m and 9 m in length. The models are usually equipped with propeller(s) and rudder(s), electrical motor, and rudder gear. Small models are subject to considerable scaling errors and usually do not yield satisfactory agreement with the full-scale ship, because the too small model Reynolds number leads to different flow separation at model hull and rudder and thus different non-dimensional forces and moments, especially the stall angle (angle of maximum lift force shortly before the flow separates completely on the suction side), which will be much smaller in models (15° to 25°) than in the full-scale ship (>35°). Another scaling error also contaminates tests with larger models: the flow velocity at the rudder outside the propeller

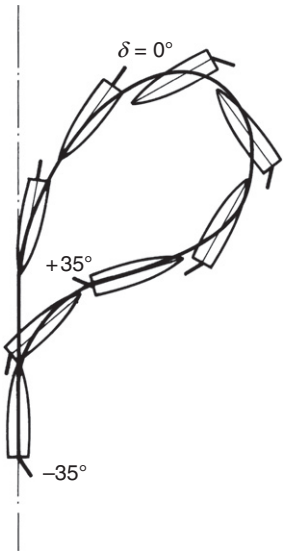

Figure 6.10:
Man-overboard maneuver (Williamson turn)

slipstream is too small (due to a too large wake fraction in model scale) and the flow velocity inside the propeller slipstream is too large (because the too large model resistance requires a larger propeller thrust). The effects cancel each other partially for single-screw ships, but usually the propeller effect is stronger. This is also the case for twin-screw twin-rudder ships, but for twin-screw midship-rudder ships the wake effect dominates for free-running models. For a captured model, propeller thrust minus thrust deduction does not have to equal resistance. Then the propeller loading may be chosen lower such that scale effects are minimized. However, the necessary propeller loading can only be estimated.

Model tests are usually performed at Froude similarity. For small Froude numbers, hardly any waves are created and the non-dimensional maneuvering parameters become virtually independent of the Froude number. For $F_n < 0.3$, for example, the body forces Y and N may vary with speed only by less than 10% for deep water. For higher speeds the wave resistance changes noticeably and the propeller loading increases, as does the rudder effectiveness if the rudder is placed in the propeller slipstream. Also, in shallow water, trim and sinkage change with F_n, influencing Y and N. If the rudder pierces the free surface or is close enough for ventilation to occur, the Froude number is always important.

Model tests with free-running models are usually performed indoors to avoid wind effects. The track of the models is recorded either by cameras (two or more) or from a carriage following the model in longitudinal and transverse directions. Turning circle tests can only be performed in broad basins and even then usually only with rather small models. Often, turning circle tests are also performed in towing tanks with an adjacent round basin at one end. The maneuver is

then initiated in the towing tank and ends in the round basin. Spiral tests and pull-out maneuvers require more space than is usually available in towing tanks. However, towing tanks are well suited for zigzag maneuvers. If the ship's track is precisely measured in these tests, all necessary body force coefficients can be determined and the other maneuvers can be numerically simulated with sufficient accuracy.

Model tests with captured models determine the body force coefficients by measuring the forces and moments for prescribed motions. The captured models are also equipped with rudders, propellers, and electric motors for propulsion.

- Oblique towing tests can be performed in a regular towing tank. For various yaw and rudder angles, resistance, transverse force, and yaw moment are measured, sometimes also the heel moment.
- Rotating arm tests were performed in a circular basin. The carriage was supported by an island in the center of the basin and at the basin edge. The carriage rotates around the center of the circular basin. The procedure is otherwise similar to oblique towing tests. Due to the disturbance of the water by the moving ship, only the first revolution could be used to measure the desired coefficients. Large non-dimensional radii of the turning circle are only achieved for small models (inaccurate) or large basins (expensive). Today, this technology is obsolete and replaced by planar motion mechanisms which can also generate accelerations, not just velocities.
- Planar motion mechanisms (PMMs) are installed on a towing carriage. They superimpose sinusoidal transverse or yawing motions (sometimes also sinusoidal longitudinal motions) to the constant longitudinal speed of the towing carriage. The periodic motion may be produced mechanically from a circular motion via a crankshaft or by computer-controlled electric motors (computerized planar motion carriage (CPMC)). The CPMC is far more expensive and complicated, but allows the extension of model motions over the full width of the towing tank, arbitrary motions and a precise measuring of the track of a free-running model.

6.4. Rudders

6.4.1. General Remarks and Definitions

Rudders are hydrofoils pivoting on a vertical or nearly vertical axis. They are normally placed at the ship's stern behind the propeller(s) to produce a transverse force and a steering moment about the ship's center of gravity by deflecting the water flow to a direction of the foil plane. Table 6.4 gives offsets of several profiles used for rudders depicted in Fig. 6.11. Other profile shapes and hydrodynamic properties are available from Abbott and Doenhoff (1959) and Whicker and Fehlner (1958).

Table 6.4: Offsets of rudder profiles

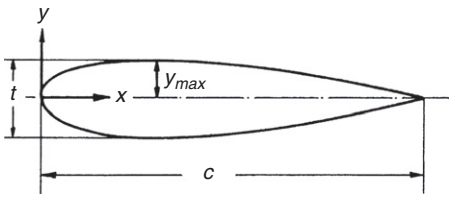

c (m) = chord length of foil
x/c (−) = dimensionless abscissa
y/c (−) = dimensionless half ordinate

Note: last digits of profile designation correspond to the thickness form, e.g. 25 for $t/c = 0.25$.
For differing thickness t_0 the half ordinates y_0 to be obtained by multiplication
$\frac{y'}{c} = \frac{t'}{t} \cdot \frac{y}{c}$

	IFS62-TR 25	IFS61-TR 25	IFS58-TR 15	HSVA-MP71-20	HSVA-MP73-20	NACA 00-20	NACA 643-018
x/c	*y/c*	*y/c*	*y/c*	*y/c*	*y/c*	*y/c*	*y/c*
0.0000	0.0000	0.0000	0.0000	0.0000	0.04420*	0.04420*	0.02208*
0.0125	0.0553	0.0553	0.0306	0.0230	0.03156	0.03156	0.02177
0.0250	0.0732	0.0732	0.0409	0.0306	0.04356	0.04356	0.03005
0.0500	0.0946	0.0946	0.0530	0.0419	0.05924	0.05924	0.04186
0.1000	0.1142	0.1142	0.0655	0.0583	0.07804	0.07804	0.05803
0.1500	0.1226	0.1226	0.0715	0.0706	0.08910	0.08910	0.06942
0.2000	**0.1250**	**0.1250**	0.0743	0.0801	0.09562	0.09562	0.07782
0.2500	0.1234	0.1226	**0.0750**	0.0881	0.09902	0.09902	0.08391
0.3000	0.1175	0.1176	0.0740	0.0939	**0.10000**	**0.10000**	0.08789
0.4000	0.0993	0.1002	0.0669	0.0996	0.09600	0.09672	**0.08952**
0.4500	—	—	—	**0.1000**	—	—	0.08630
0.5000	0.0742	0.0766	0.0536	0.0965	0.08300	0.08824	0.08114
0.6000	0.0480	0.0533	0.0377	0.0766	0.06340	0.07606	0.06658
0.7000	0.0263	0.0357	0.0239	0.0546	0.04500	0.06106	0.04842
0.8000	0.0123	0.0271	0.0168	0.0335	0.02740	0.04372	0.02888
0.9000	0.0080	0.0250	0.0150	0.0140	0.01200	0.02414	0.01101
1.0000	0.0075	0.0250	0.0150	0.0054	0.00540	0.00210	0.00000

*radius.

Rudders are placed at the ship's stern for the following reasons:

- The rudder moment turning the ship is created by the transverse force on the rudder and an oppositely acting transverse force on the ship hull acting near the bow. This moment increases with distance between the rudder force and the hull force.
- Rudders outside of the propeller slipstream are ineffective at small or zero ship speed (e.g. during berthing). In usual operation at forward speed, rudders outside of the propeller slipstream are far less effective. Insufficient rudder effectiveness at slow ship speed can be temporarily increased by increasing the propeller rpm, e.g. when passing other ships. During stopping, rudders in the propeller slipstream are ineffective.
- Bow rudders not exceeding the draft of the hull are ineffective in ahead motion, because the oblique water flow generated by the turned rudder is redirected longitudinally by the

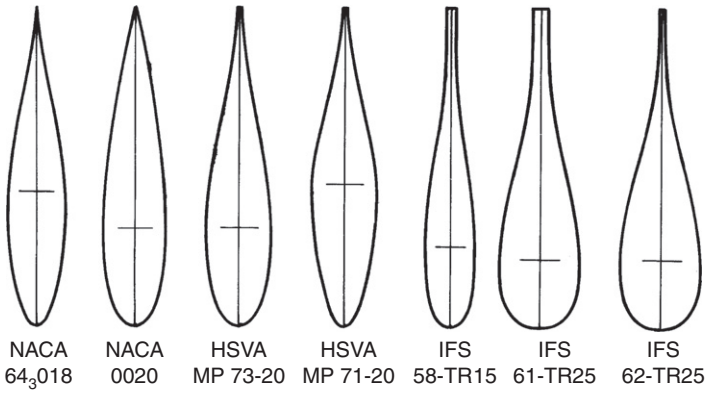

Figure 6.11:
Some rudder profiles, offsets given in Table 6.4

hull. Thus, transverse forces on a bow rudder and on the forward moving hull cancel each other. The same generally applies to stern rudders in backward ship motion. The yaw instability of the backward-moving ship in one example could not be compensated by rudder actions if the drift angle exceeded $\beta = 1.5°$. To improve the maneuverability of ships which frequently have to move astern (e.g. car ferries), bow rudders may be advantageous. In reverse flow, maximum lift coefficients of rudders range between 70% and 100% of those in forward flow. This force is generally not effective for steering the ship astern with a stern rudder, but depending on the maximum astern speed it may cause substantial loads on the rudder stock and steering gear due to the unsuitable balance of normal rudders for this condition.

The rudder effectiveness in maneuvering is mainly determined by the maximum transverse force acting on the rudder (within the range of rudder angles achievable by the rudder gear). Rudder effectiveness can be improved by:

- rudder arrangement in the propeller slipstream (especially for twin-screw ships);
- increasing the rudder area;
- better rudder type (e.g. spade rudder instead of semi-balanced rudder);
- rudder engine which allows larger rudder angles than the customary 35°;
- shorter rudder steering time (more powerful hydraulic pumps in rudder engine).

Figure 6.12 defines the parameters of main influence on rudder forces and moments generated by the dynamic pressure distribution on the rudder surface. The force components in the flow direction α and perpendicular to it are termed drag D and lift L, respectively. The moment about a vertical axis through the leading edge (nose) of the rudder (positive clockwise) is termed Q_N. If the leading edge is not vertical, the position at the mean height of the rudder is used as a reference point.

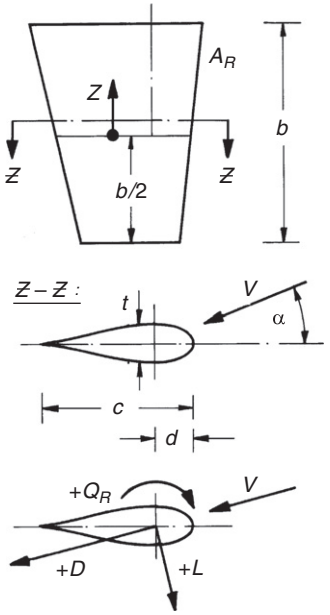

Figure 6.12:
Definition sketch of rudder geometry and rudder forces; A_R = rudder area; b = rudder height; c = chord length; d = rudder stock position; D = drag; L = lift; Q_R = rudder stock torque; t = rudder thickness; v = flow velocity; z = vertical rudder coordinate at $b/2$; α = angle of attack; δ = rudder angle; $\Lambda = b^2/A_R$ = aspect ratio

The moment about the rudder stock at a distance d behind the leading edge (nose) is:

$$Q_R = Q_N + L \cdot d \cdot \cos\alpha + D \cdot d \cdot \sin\alpha \tag{6.52}$$

The stagnation pressure $q = \frac{1}{2}\rho V^2$ and the mean chord length $c_m = A_R/b$ are used to define the following non-dimensional force and moment coefficients:

$$\text{lift coefficient} \quad C_L = L/(q \cdot A_R) \tag{6.53}$$

$$\text{drag coefficient} \quad C_D = D/(q \cdot A_R) \tag{6.54}$$

$$\text{nose moment coefficient} \quad C_{QN} = Q_N/(q \cdot A_R \cdot c_m) \tag{6.55}$$

$$\text{stock moment coefficient} \quad C_{QR} = Q_R/(q \cdot A_R \cdot c_m) \tag{6.56}$$

The stock moment coefficient is coupled to the other coefficients by:

$$C_{QR} = C_{QN} + \frac{d}{c_m}(C_L \cdot \cos\alpha + C_D \cdot \sin\alpha) \tag{6.57}$$

For low fuel consumption of the ship (for constant rudder effectiveness), we want to minimize the ratio C_L/C_D for typical small angle of attacks as encountered in usual course-keeping mode. Due to

the propeller slipstream, angles of attack of typically 10° to 15° (with opposing sign below and above the propeller shaft) occur for zero-deflected rudders. Reducing the rudder resistance by 10% in this range of angles of attack improves the propulsive efficiency by more than 1%. Various devices to improve ship propulsion by partial recovery of the propeller's rotative energy have been proposed in the course of time, e.g. Schneekluth and Bertram (1998). However, the major part of this energy is recovered anyhow by the rudder in the propeller slipstream.

Size, and thus cost, of the rudder engine are determined by the necessary maximum torque at the rudder stock. The stock moment is zero if the center of effort for the transverse rudder force lies on the rudder stock axis. As the center of effort depends on the angle of attack, this is impossible to achieve for all angles of attack. Rudder shapes with strongly changing centers of effort therefore require larger rudder engines. The position of the center of effort behind the leading edge (nose) is:

$$c_s = \frac{c \cdot C_{QN}}{C_L \cos\alpha + C_D \sin\alpha} \tag{6.58}$$

The denominator in this formula is the non-dimensional force coefficient for the normal force on the rudder.

6.4.2. Fundamental Hydrodynamic Aspects of Rudders and Simple Estimates

C_L, C_D, and C_{QN} can be determined in wind tunnel tests or computations. Extensive wind tunnel measurements have been published by Thieme (1992) and Whicker and Fehlner (1958).

Figure 6.13 shows an example. Practically these data allow rough estimates only of rudder forces and moments of ships, because in reality the flow to the rudder is irregular and highly turbulent and has a higher Reynolds number than the experiments, and because interactions with the ship's hull influence the rudder forces. For angles of attack smaller than stall angle α_s (i.e. the angle of maximum C_L) the force coefficients may be approximated with good accuracy by the following formulae:

$$C_L = C_{L1} + C_{L2} = 2\pi \frac{\Lambda \cdot (\Lambda + 0.7)}{(\Lambda + 1.7)^2} \cdot \sin\alpha + C_Q \cdot \sin\alpha \cdot |\sin\alpha| \cdot \cos\alpha \tag{6.59}$$

$$C_D = C_{D1} + C_{D2} + C_{D0} = \frac{C_L^2}{\pi \cdot \Lambda} + C_Q \cdot |\sin\alpha|^3 + C_{D0} \tag{6.60}$$

$$C_{QN} = -(C_{L1} \cdot \cos\alpha + C_{D1} \cdot \sin\alpha) \cdot \left(0.47 - \frac{\Lambda + 2}{4(\Lambda + 1)}\right) - 0.75 \cdot (C_{L2} \cdot \cos\alpha + C_{D2} \cdot \sin\alpha) \tag{6.61}$$

Figure 6.14 illustrates the C_L formula. The first term in the C_L formula follows from potential thin-foil theory for the limiting aspect ratios 0 and $\Lambda = 1$. For other aspect ratios it is an

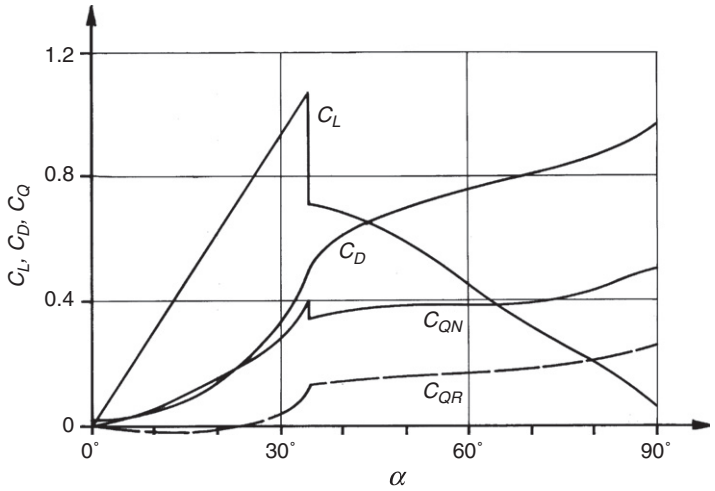

Figure 6.13:
Force and moment coefficients of a hydrofoil $\Lambda = 1$; rudder stock position $d/c_m = 0.25$; NACA-0015; $R_n = 0.79 \cdot 10^6$; Q_N = nose moment; Q_R = rudder stock torque

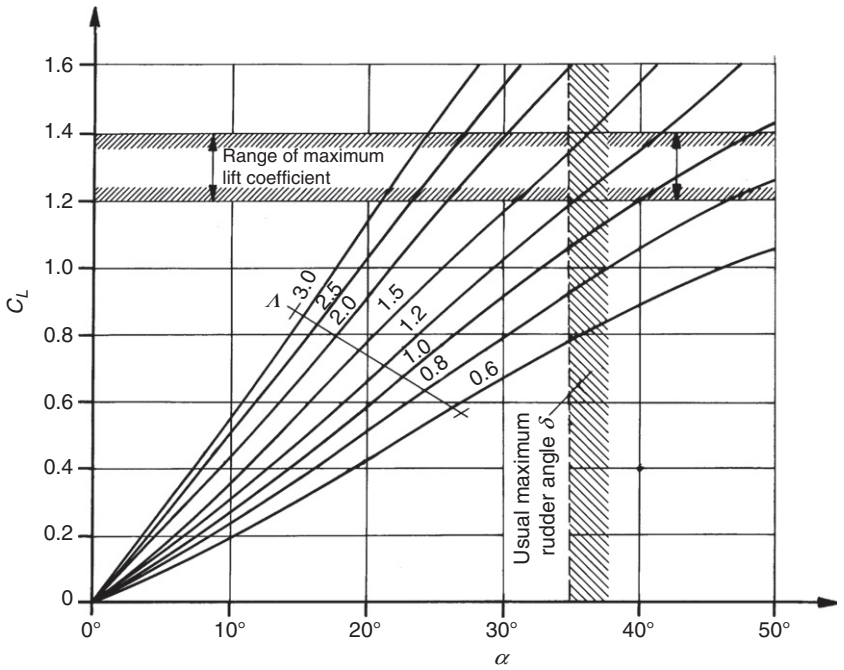

Figure 6.14:
Lift coefficient C_L versus angle of attack α with the aspect ratio Λ as parameter

approximation to theoretical and experimental results. The first term in the C_D formula is the induced resistance due to the generation of trailing vortices behind the foil. The equation includes a 10% increase in the minimum induced drag which occurs for an elliptical load distribution over the rudder height. The first term in the C_{QN} formula would be a good approximation of the theoretical moment in ideal fluid if 0.5 were used instead of the empirical value 0.47. The second terms in the formulae for C_L and C_D follow from the assumption of an additional resistance-like force depending quadratically on the velocity component $V \cdot \sin\alpha$ which is perpendicular to the rudder plane. A resistance coefficient $C_Q \approx 1$ may be used for rudders with a sharp upper and lower edge. Rounding the edges (which is difficult in practice) would lead to much smaller C_Q values. The second term in the C_{QN} formula follows from the assumption that this force component acts at 75% chord length from the leading edge. C_{D0} in the formula for C_D approximates the surface friction. We may approximate:

$$C_{D0} = 2.5 \cdot \frac{0.075}{(\log R_n - 2)^2} \tag{6.62}$$

This is 2.5 times the frictional resistance coefficient following the ITTC 1957 formula. C_{D0} refers to the rudder area which is about half the wetted area of the rudder. In addition a form factor has to be taken into account to yield the factor 2.5.

For hydrofoils the Reynolds number is defined as:

$$R_n = \frac{V \cdot c}{\nu} \tag{6.63}$$

where V is the inflow velocity (for rudders usually V_A), c the mean chord length and $\nu \approx 1.35 \cdot 10^6\ \mathrm{m^2/s}$ the kinematic viscosity of water at 10°C.

Table 6.5 shows the good agreement of the approximate formulae with model test measurements of Whicker and Fehlner (1958) (upper table) and Thieme (1962) (lower table). Thieme's results suffer somewhat from small Reynolds numbers. Rudder Reynolds numbers behind a large ship are in the vicinity of $R_n = 5 \cdot 10^7$. Too small Reynolds numbers result in larger drag coefficients, a backward shift of the center of effort of the rudder force and smaller stall angles α_s (by up to a factor of 2) than in reality. The Reynolds number of the last column in the lower table corresponds approximately to the conditions in model maneuvering experiments. However, the strong turbulence behind a ship model and its propeller act similarly to a larger Reynolds number in these experiments.

The formulae for C_L, C_D, and C_{QN} do not take into account the profile shape. The profile shape affects mainly the stall angle α_s, the maximum lift and the cavitation properties of the rudder, but hardly the lift at a given angle of attack below α_s. Table 6.5 shows that, compared to the 'standard' NACA profiles, concave profiles with thickness maximum in front of the

Table 6.5: Measured (M) and computed (C) force and moment coefficients of different profiles (Thieme 1964, Whicker and Fehlner 1958); +: independent from profile shape; *: uncertain values, probably due to experimental technique

Profile	+)	NACA 0015	+)	NACA 0015	+)	NACA 0015
Λ	1	1	2	2	3	3
$(t/c)_{max}$	+)	15	+)	15	+)	15
at x/c		30		30		30
$R_n/10^6$	2.7	2.7	2.7	2.7	2.7	2.7
Source	C	M	C	M	C	M
C_L at $\alpha = 10°$	0.27	0.27	0.44	0.44	0.55	0.55
C_L at $\alpha = 20°$	0.59	0.60	0.92	0.93	1.14	1.10
C_L at $\alpha = \alpha_s$	1.17	1.26	1.33	1.33	1.32	1.25
α_s (°)	38.5	38.5	28.7	28.7	23.0	23.0
C_L/C_D at $\alpha = 10°$	8.11	7.26	10.45	10.35	12.28	12.40
C_L/C_D at $\alpha = 20°$	4.62	4.25	5.70	5.79	6.63	7.05
C_L/C_D at $\alpha = \alpha_s$	2.28	2.20	3.88	4.00	5.76	6.00
c_s/c at $\alpha = 10°$	0.17	0.16	0.18	0.19	0.19	0.18
c_s/c at $\alpha = \alpha_s$	0.30	0.31	0.24	0.25	0.23	0.23

Profile	NACA 0015	NACA 0025	IFS62 TR 25	IFS61 TR 25	IFS58 TR 15	Plate t/c = 0.03	NACA 0015
Λ	1	1	1	1	1	1	1
$(t/c)_{max}$	15	25	25	25	15	3	15
at x/c	30	30	20	20	25	–	30
$R_n/10^6$	0.79	0.78	0.78	0.79	0.79	0.71	0.20
Source	M	M	M	M	M	M	M
C_L at $\alpha = 10°$	0.29	0.27	0.33	0.32	0.32	0.34	0.35
C_L at $\alpha = 20°$	0.62	0.59	0.71	0.69	0.67	0.72	0.55
C_L at $\alpha = \alpha_s$	1.06	1.34	1.48	1.34	1.18	1.14	0.72
α_s (°)	33.8	46.0*	46.0*	41.0*	33.5	40*	35.0*
C_L/C_D at $\alpha = 10°$	7.20	5.40	4.70	4.00	6.40	3.80	2.80
C_L/C_D at $\alpha = 20°$	4.40	4.20	3.60	3.60	3.90	2.50	1.75
C_L/C_D at $\alpha = \alpha_s$	2.30	1.70	1.50	1.80	2.40	1.30	1.19
c_s/c at $\alpha = 10°$	0.18	0.20	0.27	0.26	0.25	0.28	0.28
c_s/c at $\alpha = \alpha_s$	0.35	0.35	0.36	0.25	0.33	0.41	0.43

standard value of 30% of the chord length (measured from the leading edge) produce larger maximum lift and less change of the center of effort of the rudder force. The latter fact allows a smaller steering gear if the rudder is properly balanced. On the other hand, these profiles have higher drag coefficients, thus requiring more propulsive power for the same ship speed. (For a rudder behind a propeller, the slipstream rotation causes angles of attack of typically 10° to 15°.) A 10% increase of the rudder resistance in this angle-of-attack range accounts for approximately 1% increase in the necessary propulsion power. For ship speeds exceeding 22 knots and the rudder in the propeller slipstream, profiles with the opposite

tendency (backward-shifted maximum thickness) are preferred because they are less prone to cavitation.

Greater profile thickness produces greater maximum lift at the (correspondingly greater) stall angle α_s, but it increases the rudder drag, and in most cases the danger of cavitation in high-speed ships. Thus, the smallest thickness possible to accommodate the rudder post and bearing is normally used. For rudders of small aspect ratio, the greater maximum lift of thick rudders is realized only in yaw checking, but not at all if the steering gear allows the normal $\delta = 35°$ rudder angle only (Fig. 6.14). A trailing edge of substantial thickness decreases the change of the center of effort c_s with angle of attack α, but it causes substantially increased drag; thus, because of too large drag, the application of these profiles should be avoided, at least in long-range vessels.

The approximate formulae for the force coefficients are only valid for angles of attack $\alpha < \alpha_s$. Beyond the stall angle α_s the flow separates near the profile leading edge (nose) on the suction side of the profile without reattachment. Then the lift decreases strongly and the drag increases (Fig. 6.13). The sudden drop in lift beyond the stall angle α_s is not found for certain other profiles and in rudders behind a propeller.

The stall angle α_s depends primarily on:

- the aspect ratio Λ;
- the profile shape and thickness;
- the Reynolds number;
- probably the surface roughness;
- the turbulence of the inflow;
- the spatial distribution of the inflow velocity.

Because of the last four parameters, an exact prediction of maximum rudder lift from wind tunnel or towing tank experiments is impossible. Whereas a greater aspect ratio Λ (height-to-chord ratio b/c_m) increases the lift for a given angle of attack $\alpha < \alpha_s$, the maximum lift coefficient is practically independent of the aspect ratio (Fig. 6.14). Thus increasing the rudder area by increasing the chord length is of equal effect as by increasing the rudder height with respect to the maximum rudder force if the stall angle is reached by the steering gear; otherwise, an increase in rudder height is much more effective than a corresponding increase in chord length. (A rudder angle $\delta = 35°$ relative to the ship's longitudinal axis corresponds to angles of attack α_s, of nearly the same size in initial turning, of smaller size during steady turning and of larger size in the yaw checking phase.)

Because of the different stall angles α_s and lift curve slopes of rudders of different aspect ratios it would be advantageous to use an effective rudder angle δ_{eff} instead of the geometrical rudder angle δ for rules, e.g. about the maximum rudder angle and the rudder rate of the steering gear, as well as for nautical use. This would be 'fairer' for rudders of different aspect ratio; it would also

make better use of rudders of smaller aspect ratio (today their greater stall angle α_s is frequently not realized because of a too small maximum rudder angle δ) and would lead to more equal response of different ships on (effective) rudder angles. If geometric and effective rudder angles are defined to coincide for a normal aspect ratio of $\Lambda = 2$, their relationship is (Fig. 6.15):

$$\delta_{\text{eff}} = \frac{2.2 \cdot \Lambda}{\Lambda + 2.4} \cdot \delta \tag{6.64}$$

For aspect ratios $\Lambda < 3$, which are typical for ship rudders, the vertical distribution of the lift force in homogeneous, unbounded flow is practically elliptic:

$$\text{lift per length} = \frac{L}{b} \cdot \frac{4}{\pi} \cdot \sqrt{1 - \left(\frac{z}{b/2}\right)^2} \tag{6.65}$$

Here z is the vertical distance from the mean height between the lower and upper edges of the rudder. The distribution is hardly influenced by the rudder shape for the usual trapezoidal shape with a taper ratio $0.5 < c_{\min}/c_{\max} < 1.0$. Thus, for a free-running rudder of trapezoidal shape the lift center is nearly at half the rudder height, not at the center of gravity of the shape. This effect is even more pronounced for lower aspect ratios. If there is only a small gap between the upper edge of the rudder and fixed parts of the hull (at the rudder angles concerned), the center of effort moves up a little, but never more than 7.5% of b, the value for a rudder without a gap at its upper edge.

Air ventilation may occur on the suction side of the rudder if the rudder pierces or comes close to the water surface. The extent of the ventilation may cover a large part of the rudder (even the

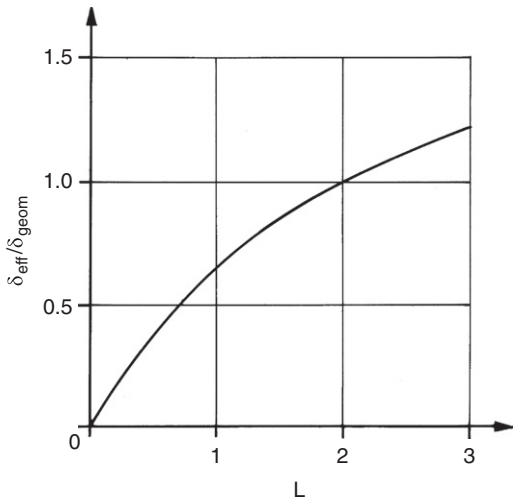

Figure 6.15:
Ratio between effective and geometrical angles of attack

whole rudder height), decreasing the rudder effectiveness drastically. This is important for maneuvers at ballast draft for full speed, e.g. at ship trials.

The dynamic pressure along the profile of a rudder depends on the local velocity v according to Bernoulli's law:

$$p_{\text{dyn}} = \frac{\rho}{2} \cdot \left(V^2 - v^2\right) = q \cdot \left(1 - \frac{v^2}{V^2}\right) \tag{6.66}$$

For the usual straight profiles v/V is decomposed into two components:

1. Component v_t/V due to the profile thickness t. This component is equal on both sides of the profile. v_t/V may be taken from Table 6.6. For different profile thickness t, the velocity ratio v_t/V must be corrected by

$$\left[\left(\frac{v_t}{V}\right)_{\text{actual}} - 1\right] = \left[\left(\frac{v_t}{V}\right)_{\text{table}} - 1\right] \cdot \frac{t_{\text{actual}}}{t_{\text{table}}} \tag{6.67}$$

   Information on other profiles may be found in Abbott and Doenhoff (1959) or computed by CFD (e.g. boundary element method).
2. Component v_a/V due to the angle of attack α_s. This component has opposite sign on both sides of the profile. It is practically independent of the profile shape. Only in the front part

Table 6.6: $v_t = V$; flow speed v_t along the profile over inflow velocity V as a function of the profile abscissa x, $\alpha = 0^\circ$

x/c (%)	NACA 643-018	NACA 0020	HSVA MP73-20	HSVA MP71-20	IFS58 TR15	IFS61 TR25	IFS62 TR25
0	0.00	0.00	0.00	0.00	0.00	0.00	0.00
0.75	0.77	0.69	0.69	0.57	0.79	0.67	0.68
1.25	0.96	0.91	0.91	0.88	1.06	0.95	0.94
2.5	1.05	1.03	1.08	1.00	1.20	1.09	1.18
6.0	1.11	1.17	1.22	1.10	1.29	1.47	1.48
7.5	1.15	1.25	1.27	1.12	1.30	1.52	1.53
10	1.17	1.27	1.29	1.14	1.28	1.50	1.52
15	1.20	1.30	1.31	1.18	1.26	1.47	1.48
20	1.22	1.29	1.30	1.20	1.23	1.43	1.44
30	1.25	1.26	1.27	1.24	1.20	1.31	1.33
40	1.26	1.21	1.24	1.28	1.16	1.18	1.21
50	1.20	1.17	1.17	1.30	1.08	1.06	1.08
60	1.13	1.13	1.07	1.14	1.00	0.96	0.97
70	1.06	1.08	1.01	1.04	0.94	0.90	0.90
80	0.98	1.03	0.95	0.96	0.93	0.90	0.87
90	0.89	0.96	0.88	0.87	0.96	0.94	0.90
95	0.87	0.91	0.89	0.87	0.97	0.95	0.93

does it depend on the profile nose radius. Figure 6.16 illustrates this for a lift coefficient $C_{Ll} \approx 1$. The values given in Fig. 6.16 have to be multiplied by the actual local lift coefficient:

3.

$$C_{Ll} = \frac{\text{lift per length}}{c \cdot q} = C_L \cdot \frac{4}{\pi} \cdot \sqrt{1 - \left(\frac{z}{b/2}\right)^2} \tag{6.68}$$

where $C_L(\Lambda)$ is estimated by Eq. (6.59).

The dynamic pressure is then:

$$p_{\text{dyn}} = \left[1 - \left(\frac{v_t}{V} \pm \frac{v_a}{V} \cdot C_{Ll}\right)^2\right] \cdot q \tag{6.69}$$

Due to the quadratic relationship in this equation, the pressure distribution will generate the given C_{Ll} only approximately. For better accuracy, the resulting local lift coefficient should be integrated from the pressure difference between both sides of the profile. If it differs substantially from the given value, the pressure distribution is corrected by superimposing the v_a/V distribution in Eq. (6.69) with a factor different from C_{Ll} such that the correct C_{Ll} is attained by the integration of the pressure difference.

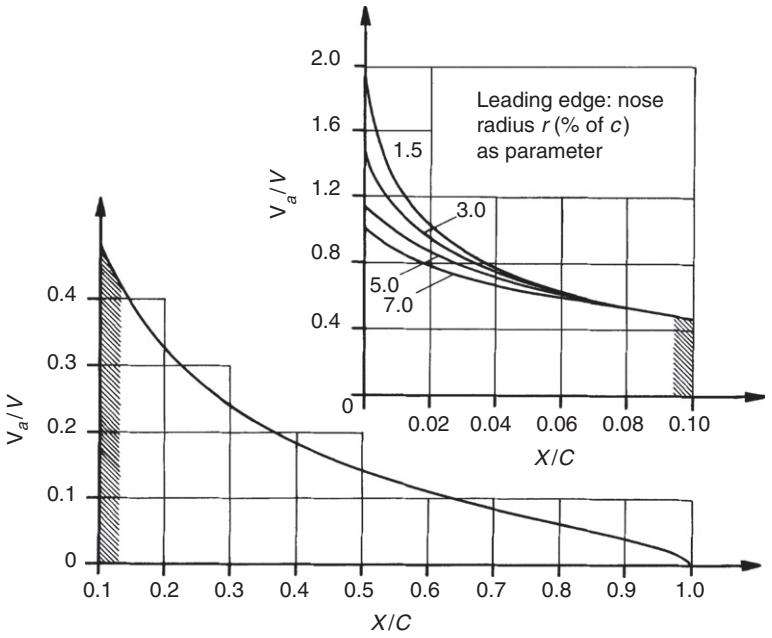

Figure 6.16:
Relative change of velocity v_a/V on the surface due to the angle of attack α_s for $C_{Ll} \approx 1$

The dynamic pressure is negative over most of the profile length, for moderate lift coefficients even on the pressure side of the rudder. This is illustrated in Fig. 6.17 for an NACA0021 profile. The curve for $C_{Ll} = 0$ corresponds to the component due to the profile thickness alone. For other C_{Ll} values, the upper and lower curves refer to the pressure and suction sides, respectively. For profiles with a curved mean line, an additional velocity component has to be added. It may be taken from Abbott and Doenhoff (1959, pp. 77ff and App. II), or it may be determined by a two-dimensional potential-flow calculation for which various methods and codes are available. Brix (1993, p. 84) gives a sample calculation for the NACA643-018 profile for $\alpha = 15°$.

6.4.3. Rudder Types

Various rudder types have been developed over the years (Fig. 6.18):

- *Rudder with heel bearing (simplex)*
  The most common rudder type formerly built was a rectangular profile rudder with heel bearing. The heel has to have considerable width to withstand the horizontal forces. Flow separation at the heel increases resistance and the non-homogeneity of the wake field at the propeller plane, which in turn increases propeller-induced vibrations. Therefore modern single-screw ships are usually equipped with other rudder types, but the rudder with heel bearing is still popular for small craft and some fishery vessels, because it is cheap.

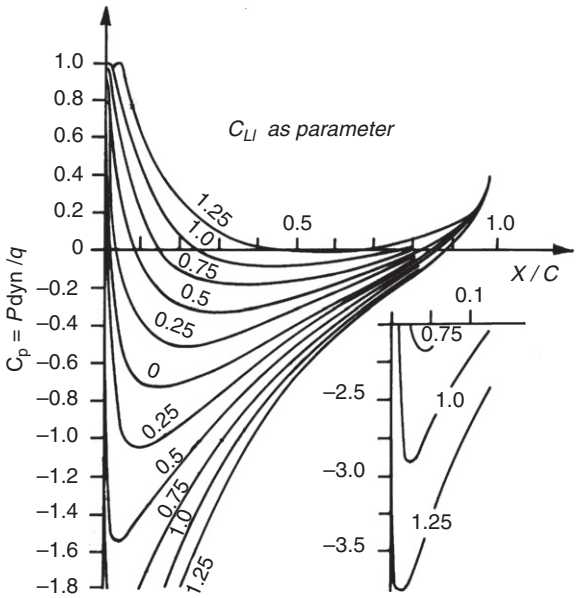

Figure 6.17:
Distribution of the non-dimensional dynamic pressure along an NACA0021 profile as a function of the local lift coefficient C_{Ll} (Riegels 1958)

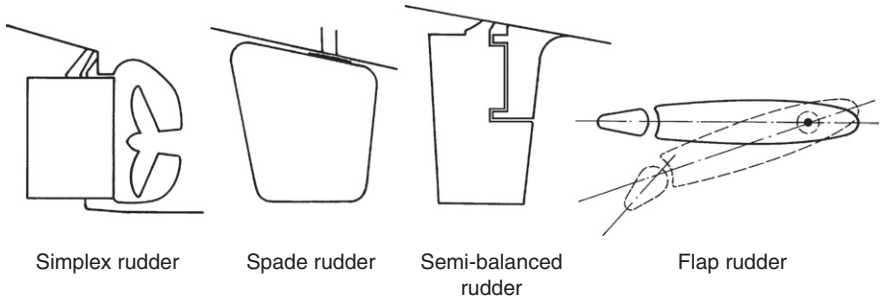

Figure 6.18:
Various rudder types

- *Spade rudder*
  This type of rudder is commonly applied, especially on ferries, ro-ro ships, and special craft. The rudder stock is subject to high bending moments, especially for high ship speed and large rudder height. For stock diameters larger than 1 m, this design becomes impractical.
- *Semi-balanced rudders*
  For semi-balanced rudders, a fixed guide-head (sometimes called rudder horn) extends over the upper part of the rudder. This type of rudder has the following properties:
  - Decreased rudder bending moment compared to spade rudders.
  - Reduced rudder effectiveness compared to spade rudders. For steady turning circles, the semi-balanced rudder produces only approximately half the transverse force as a spade rudder of the same area (including the area of the rudder horn). The reasons for the reduced transverse force are:
    - The horizontal gap between horn and rudder opens wide for large rudder angles. Sometimes horizontal plates are attached at the horn along the gap as a remedy for this problem (rudder scissors).
    - Unfavorable angle of attack for the rudder horn (fixed guide-head).
    - Drag/lift ratio of the rudder about twice as high as for spade rudders.
- *Flap rudders*
  Flap rudders (e.g. Becker rudders) consist of a movable rudder with a trailing edge flap activated by a mechanical or hydraulical system, thus producing a variable flap angle as a function of the rudder angle. This system works like an airfoil with a flap. Flap rudders give a much higher lift per rudder angle and a 60−70% higher maximum lift compared to a conventional rudder of the same shape, size, and area.

Less frequently, the following rudder types are employed:

- *Rudders with rotating cylinders*
  These rudders have a rotating cylinder at the leading edge. Whereas the freely arranged rotating cylinder works according to the Magnus effect, the combination of a rotating cylinder and a conventional rudder shifts the stall to a much higher angle of attack by eliminating the

boundary layer at the separation-prone leading edge. However, at full scale the stall angle of conventional rudders is often so high that the added complexity of this rudder is not justified.

- *Active rudder/rudder propellers*
  Rudder propellers are azimuthing ducted or free-running propellers in a fixed or hinged vertical position. They are active control devices with directed thrust. The 'active propeller' is a special solution of a motor-driven ducted propeller integrated in the main rudder. Thus, besides auxiliary propulsion qualities, a directed thrust is available within the range of the main rudder angles. This increases the maneuvering qualities of the ship, especially at low speeds.
- *Steering nozzle with rudder*
  Steering nozzle may be fitted with flapped or unflapped rudders. This highly effective steering device is sometimes fitted to tugs, or research or fishery ships.

A fixed fin above the rudder improves the yaw checking stability as much as if the area of the fixed fin were included in the movable rudder. However, for course-changing ability only the movable rudder is decisive. In fact, a fixed fin has a course-stabilizing property and increases, for example, the turning circle diameter. A gap between the rudder top and the hull increases the rudder resistance at center position due to the induced resistance of the oblique inflow of the propeller slipstream and the resistance of the rudder.

Twin-screw ships may be fitted with spade or semi-balanced rudders, either behind the propellers or as midship rudders. For fast ships with a rudder arrangement on the centerplane cavitation problems are avoided, but this arrangement is less effective than rudders in the propeller slipstream, especially on shallow water.

6.4.4. Interaction of Rudder and Propeller

Rudders are normally placed in the propeller slipstream for the following reasons:

- A profiled rudder increases the propulsive efficiency by utilizing a part of the rotational energy contained in the propeller slipstream.
- In steady ahead motion, the rudder forces are typically more than twice those of a rudder outside of the propeller slipstream.
- Even for a stationary or slowly moving ship, substantial rudder forces may be generated by increasing the propeller rpm (especially to provide increased rudder effectiveness during transient maneuvers).

Because the rudder forces are proportional to the flow speed squared at the rudder, an accurate determination of the speed in the propeller slipstream at the rudder position is required to correctly predict rudder forces. According to the momentum theory of the propeller, the mean axial speed of the slipstream far behind the propeller is:

$$V_\infty = V_A\sqrt{1+C_{Th}} \tag{6.70}$$

where C_{Th} is the thrust loading coefficient according to Eq. (2.5). V_A is the mean axial speed of inflow to the propeller, A_P the propeller area. The theoretical slipstream radius r_∞ far behind the propeller flows from the law of continuity, assuming that the mean axial speed at the propeller is the average between V_A and V_∞:

$$r_\infty = r_0\sqrt{\frac{1}{2}\left(1+\frac{V_A}{V_\infty}\right)} \tag{6.71}$$

Here r_0 is half the propeller diameter D.

Normally the rudder is in a position where the slipstream contraction is not yet completed. The slipstream radius and axial velocity may be approximated by (Söding 1982):

$$r = r_0 \cdot \frac{0.14(r_\infty/r_0)^3 + r_\infty/r_0 \cdot (x/r_0)^{1.5}}{0.14(r_\infty/r_0)^3 + (x/r_0)^{1.5}} \tag{6.72}$$

and

$$V_x = V_\infty \cdot \left(\frac{r_\infty}{r}\right)^2 \tag{6.73}$$

Here x is the distance of the respective position behind the propeller plane. To determine rudder force and moment, it is recommended to use the position of the center of gravity of the rudder area within the propeller slipstream.

The above expression for r is an approximation of a potential-flow calculation. Compared to the potential flow result, the slipstream will increase in diameter with increasing distance x from the propeller plane due to turbulent mixing with the surrounding fluid. This may be approximated (Söding 1986) by adding:

$$\Delta r = 0.15x \cdot \frac{V_x - V_A}{V_x + V_A} \tag{6.74}$$

to the potential slipstream radius and correcting the slipstream speed according to the momentum theorem:

$$V_{\text{corr}} = (V_x - V_A)\left(\frac{r}{r+\Delta r}\right)^2 + V_A \tag{6.75}$$

The results of applying this procedure are shown in Fig. 6.19. V_{corr} is the mean value of the axial speed component over the slipstream cross-section.

The rudder generates a lift force by deflecting the water flow up to considerable lateral distances from the rudder. Therefore the finite lateral extent of the propeller slipstream

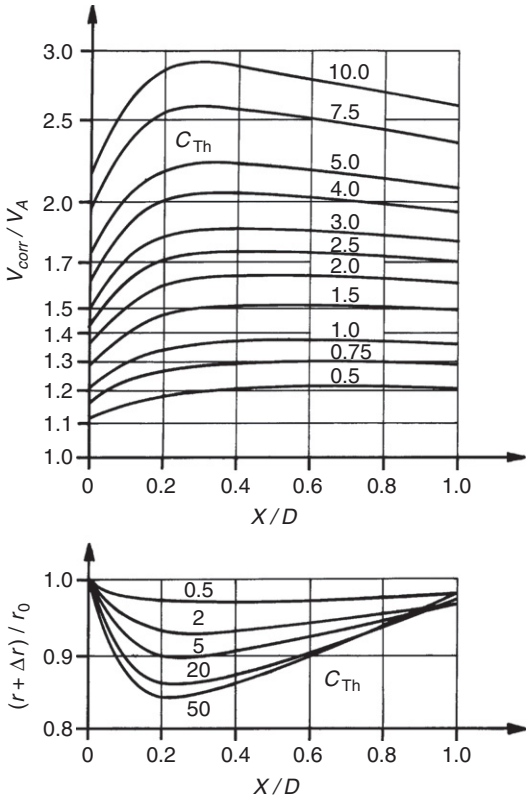

Figure 6.19:
Mean axial slipstream speed as a function of propeller approach speed V_A and slipstream radius $(r + \Delta r)/r_0$ due to potential flow and turbulent mixing at different positions x/D behind the propeller

diminishes the rudder lift compared to a uniform inflow velocity. This is approximated (Söding 1982) (based on two-dimensional potential flow computations for small angles of attack) by multiplying the rudder lift determined from the velocity within the rudder plane by the correction factor λ determined from:

$$\lambda = \left(\frac{V_A}{V_{\text{corr}}}\right)^f \quad \text{with} \quad f = 2 \cdot \left(\frac{2}{2 + d/c}\right)^8 \tag{6.76}$$

Here V_A is the speed outside of the propeller slipstream laterally from the rudder. d is the half-width of the slipstream. For practical applications, it is recommended to transform the circular cross-section (radius $r + \Delta r$) of the propeller slipstream to a quadratic one (edge length $2d$) of equal area. This leads to the relation:

$$d = \sqrt{\frac{\pi}{4}}(r + \Delta r) = 0.886 \cdot (r + \Delta r) \tag{6.77}$$

The inflow velocity in the rudder plane varies along the rudder height due to the wake distribution and the propeller slipstream. The effect of this variation may be approximated by using the mean squared velocity:

$$\overline{V^2} = \frac{1}{A_R} \int_0^b V^2 \cdot c \, \mathrm{d}z \tag{6.78}$$

for the determination of the rudder lift.

Lifting-surface calculations show that, compared to a uniform distribution, the lift coefficient (defined with reference to $\overline{V^2}$) is some 5% higher for rudders extending downward beyond the lower edge of the propeller slipstream (Fig. 6.20). Hence it is recommended to extend the rudder as far to the baseline of the ship as possible.

A simple global correction for the lift force of a rudder behind a propeller (to be added to the lift computed by the usual empirical formulae for rudders in free stream) is (Söding 1998a, b):

$$\Delta L = T \cdot \left(1 + \frac{1}{\sqrt{1 + C_{Th}}}\right) \cdot \sin \delta \tag{6.79}$$

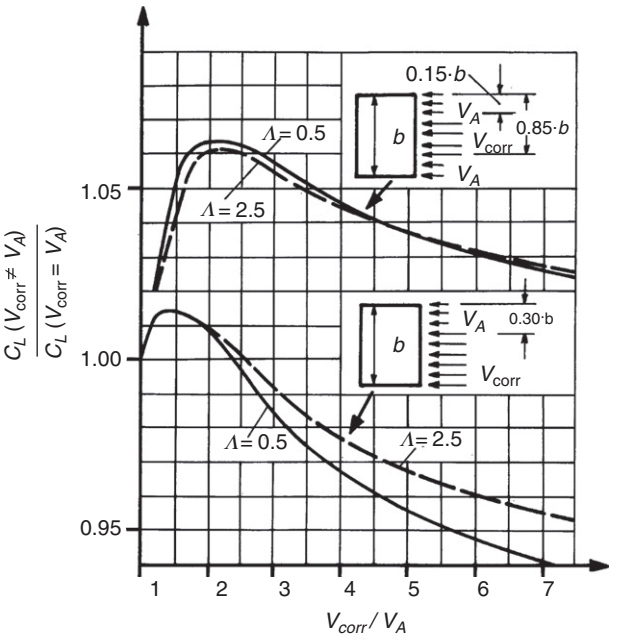

Figure 6.20:
Lift coefficients as a function of the vertical distribution of flow and the aspect ratio Λ

The additional drag (or decrease in propeller thrust) is:

$$\Delta D = T \cdot \left(1 + \frac{1}{\sqrt{1 + C_{Th}}}\right) \cdot (1 - \cos \delta) \tag{6.80}$$

In these formulae, T denotes the propeller thrust.

6.4.5. Interaction of Rudder and Ship Hull

If the hull above the rudder is immersed, it suppresses the flow from the pressure to the suction side around the upper edge of the rudder. This has effects similar to an increase of the rudder aspect ratio Λ:

- It decreases the induced drag.
- It increases the slope of the lift curve versus angle of attack α.
- It hardly influences the maximum lift at the stall angle α_s.

The magnitude of this effect depends on the size of the gap between the upper edge of the rudder and the hull. For very small gaps, the aspect ratio Λ_{eff} is theoretically twice the nominal value, in practice $\Lambda_{\text{eff}} \approx 1.6 \cdot \Lambda_{\text{geom}}$. To close the gap between hull and rudder at least for small rudder angles δ – and thus increasing the rudder effectiveness – a fixed fin above the rudder is advantageous for small rudder angles. If the hull above the rudder is not immersed or if the rudder intersects the water surface, the free surface may also increase somewhat the effective aspect ratio Λ_{eff}. However, this effect decreases with increasing ship speed and may turn to the opposite at higher speed by rudder ventilation drawn from the surface along the suction side of the rudder. To decrease rudder ventilation, a broad stern shape sufficiently immersed into the water, especially above the front part of the rudder, is advantageous.

The wake of the hull decreases the inflow velocity to the rudder and increases the propeller load. Differences in wake and propeller load between model and ship are the main cause of scale effects in model maneuvering experiments. Whereas the wake due to hull surface friction will be similar at the rudder and at the propeller, the potential wake – at least for small Froude numbers, i.e. without influence of the free surface – is nearly zero at the rudder, but typically amounts to 10–25% of the ship's speed at the propeller of usual single-screw ships. It amounts nearly to the thrust deduction fraction t. Thus the flow outside of the propeller slipstream is accelerated between the propeller and the rudder by about $t \cdot V$. This causes a pressure drop which also accelerates the propeller slipstream to approximately:

$$V_x = \frac{V_{\text{corr}}^2 + t \cdot V^2}{V_{\text{corr}}} \tag{6.81}$$

The corresponding slipstream contraction is:

$$r_x = (r + \Delta r) \cdot \sqrt{\frac{V_{\text{corr}}}{V_x}} \tag{6.82}$$

For non-zero rudder angle and forward ship speed, an interaction between the flow around rudder and hull occurs which decreases the lift force at the rudder; however, an additional transverse force of equal direction is generated at the aftbody. Compared to the rudder lift without hull interaction, the total transverse force is increased by the factor $(1 + a_H)$. The term a_H may be approximated (Söding 1982):

$$a_H = \frac{1}{1 + (4.9 \cdot e/T + 3c/T)^2} \tag{6.83}$$

Here T is the draft of the ship, e the mean distance between the front edge of the rudder and the aft end of the hull, and c the mean rudder chord length. Compared to the free-running rudder, the center of effort of the total transverse force is shifted forward by approximately:

$$\Delta x = \frac{0.3T}{e/T + 0.46} \tag{6.84}$$

Potential flow computations show that Δx may increase to up half the ship's length in shallow water if the gap length e between rudder and hull tends to zero, as may be the case for twin-screw ships with a center rudder. This would decrease the ship's turning ability on shallow water. For a non-zero drift velocity v (positive to starboard, measured amidships) and a non-zero yaw rate r (positive clockwise if seen from above) of the ship, the hull in front of the rudder influences the flow direction at the rudder position. Without hull influence, the transverse flow velocity v relative to the hull at the rudder position x_R is:

$$v_R = -(v + x_R \cdot r) \tag{6.85}$$

x_R is the distance between rudder and midship section, negative for stern rudders. However, experiments of Kose (1982) with a freely rotating, unbalanced rudder behind a ship model without propeller indicated a mean transverse velocity at the rudder's position of only:

$$v_R = -(0.36 \cdot v + 0.66 \cdot x_R \cdot r) \tag{6.86}$$

From the rudder angle δ (positive to port side), the mean longitudinal flow speed V_x (positive backward) and the mean transverse flow speed v_R at the rudder position, the angle of attack follows:

$$\alpha = \delta + \arctan\frac{v_R}{V_{\text{corr}}} \tag{6.87}$$

6.4.6. Rudder Cavitation

Rudder cavitation may occur even at small rudder angles for ship speeds exceeding 22 knots with rudder(s) in the propeller slipstream and $P/A_P > 700\,\text{kW/m}^2$. Here P is the delivered power, A_P the propeller disk area.

Rudder cavitation — as with propeller cavitation — is caused by water evaporation where at points of high flow velocity the pressure locally drops below the vapor pressure of the water. Cavitation erosion (loss of material by mechanical action) occurs when small bubbles filled with vapor collapse on or near to the surface of the body. During the collapse a microscopic high-velocity jet forms, driven by surface tension and directed onto the body surface. It causes small cracks and erosion, which in seawater may be magnified by corrosion (galvanic loss of material). Paint systems, rubber coatings, enamel, etc. offer no substantial resistance to cavitation, but austenitic steel and some types of bronze seem to retard the erosion compared to the mild steel normally used for rudders.

The cavitation number σ (Fig. 6.21) is a non-dimensional characteristic value for studying cavitation problems in model experiments:

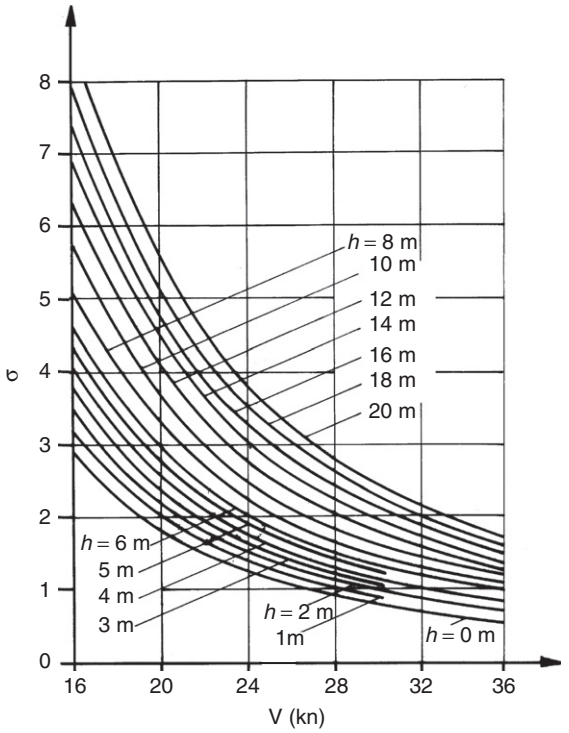

Figure 6.21:
Cavitation number σ as a function of the ship speed V with the submersion h (depth below water surface) as parameter

$$\sigma = \frac{p - p_v}{1/2 \rho V^2} \tag{6.88}$$

p is the pressure in undisturbed flow, i.e. atmospheric pressure plus hydrostatic pressure, p_v vaporization pressure, V ship speed, ρ density of water.

There are different types of rudder cavitation:

1. *Bubble cavitation on the rudder side plating*
   For large rudder angles, cavitation is unavoidable in ships of more than about 10 knots. It will decrease the rudder lift substantially if the cavitation causes a complete separation of flow from the suction side. Otherwise its influence on rudder forces is small (Kracht 1987). Cavitation erosion is of interest only if it occurs within the range of rudder angles $\delta = \pm 5°$ used for course keeping. Evaluation of model experiments shows that the onset of cavitation is indeed observed if the pressure determined by potential-flow theory is smaller than the water vaporization pressure p_v. p_v lies typically between 1% and 3% of the atmospheric pressure. It may therefore (not in model tests, but for full-scale ships) simply be taken as zero. Thus, to test for blade side cavitation in the design stage of ships, one may proceed as follows:
   - Determine the slipstream radius $r + \Delta r$ and the inflow speed to the rudder V_{corr} from Fig. 6.19 or the corresponding formulae at about 80% of the propeller tip radius above and below the propeller axis.
   - Correct these values to obtain V_x and r_x by Eqs (6.81) and (6.82).
   - Because of non-uniform distribution of the slipstream velocity, add 12% of V to obtain the maximum axial speed at the rudder:

$$V_{\max} = V_x + 0.12 \cdot (V_{\text{corr}} - V_A) \tag{6.89}$$

   - Estimate the inflow angle α to the rudder due to the rotation of the propeller slipstream by:

$$\alpha = \arctan\left(4.3 \cdot \frac{K_Q}{J^2} \cdot \sqrt{\frac{1 - \overline{w}}{1 - w_{\text{local}}}} \cdot \frac{V_A}{V_{\max}}\right) \tag{6.90}$$

     $\overline{w}$ is the mean wake number and w_{local} the wake number at the respective position. The equation is derived from the momentum theorem with an empirical correction for the local wake. It is meant to apply about 0.7 to 1.0 propeller diameter behind the propeller plane. The position relevant to the pressure distribution is about one-half chord length behind the leading edge of the rudder.
   - Add $\delta = 3° = 0.052$ rad as an allowance for steering rudder angles.
   - Determine the maximum local lift coefficient $C_{Ll\max}$ from Fig. 6.22, where $\alpha + \delta$ are to be measured in radians. c is the chord length of the rudder at the respective height,

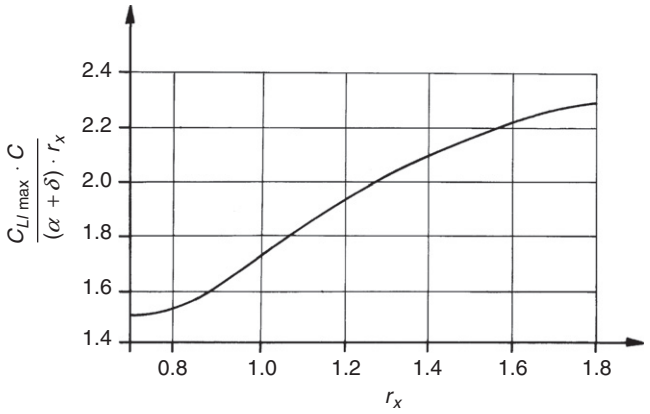

Figure 6.22:
Diagram for determining the local values of maximum lift coefficient $C_{Al\max}$

r_x the propeller slipstream radius following from Eq. (6.70) with r_x in the place of r_∞. Figure 6.22 is based on lifting-line calculations of a rudder in the propeller slipstream. It takes into account the dependence of the local lift coefficient on the vertical variation of inflow velocity and direction.

- Determine the extreme negative non-dimensional pressure on the suction side depending on profile and local lift coefficient $C_{Al\max}$. For this we use Fig. 6.23 derived from potential flow calculations.
- Add to p_{dyn} (negative) the static pressure $p_{stat} = 103\,\text{kPa} + \rho \cdot g \cdot h$. h is the distance between the respective point on the rudder and the water surface, e.g. 80% of the propeller radius above the propeller axis.

If the resulting minimum pressure on the suction side is negative or slightly positive (less than 3 kPa), the side plating of the rudder is prone to cavitation. For a right-turning propeller (turning clockwise looking forward) cavitation will occur:

- on the starboard side in the upper part of the rudder relative to the propeller axis;
- on the port side in the lower part of the rudder relative to the propeller axis.

Brix (1993, pp. 91–92) gives an example for such a computation. Measures to decrease rudder side cavitation follow from the above prediction method:

- Use profiles with small p_{dyn} at the respective local lift coefficient. These profiles have their maximum thickness at approximately 40% behind the leading edge.
- Use profiles with an inclined (relative to the mean rudder plane) or curved mean line to decrease the angle of attack (Brix et al. 1971). For a right-turning propeller, the rudder nose should be on the port side above the propeller axis, on the starboard side below it.

2. *Rudder sole cavitation*

Due to the pressure difference between both sides of the rudder caused, say, by the rotation of the propeller slipstream, a flow component around the rudder sole from the pressure to

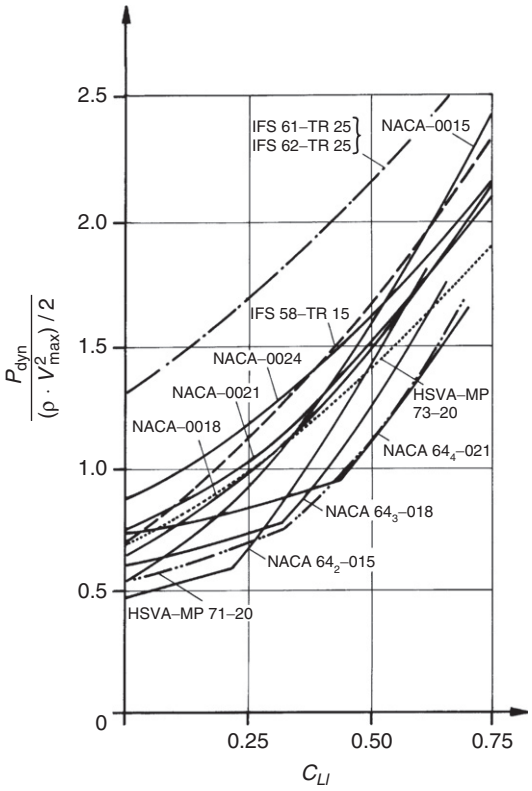

Figure 6.23:
Extreme negative dynamic pressure of the suction side as a function of the local lift coefficient C_{LI} and the profile

the suction side occurs. It causes a rudder tip vortex (similar to propeller tip vortices) which may be filled by a cavitation tube. This may cause damage if it attaches to the side of the rudder. However, conditions for this are not clear at present. If the rudder has a sharp corner at the front lower edge, even for vanishing angles of attack the flow cannot follow the sharp bend from the leading edge to the base plate, causing cavitation in the front part of the rudder sole. As a precaution the base plate is bent upward at its front end (Brix et al. 1971). This lowers the cavitation number below which sole cavitation occurs (Fig. 6.24). For high ship speeds exceeding, say, 26 knots cavitation has still been reported. However, it is expected that a further improvement could be obtained by using a smoothly rounded lower face or a baffle plate at the lower front end (Kracht 1987). No difficulties have been reported at the rudder top plate due to the much lower inflow velocity.

3. *Propeller tip vortex cavitation*
Every propeller causes tip vortices. These are regions of low pressure, often filled with cavitation tubes. Behind the propeller they form spirals which are intersected by the rudder.

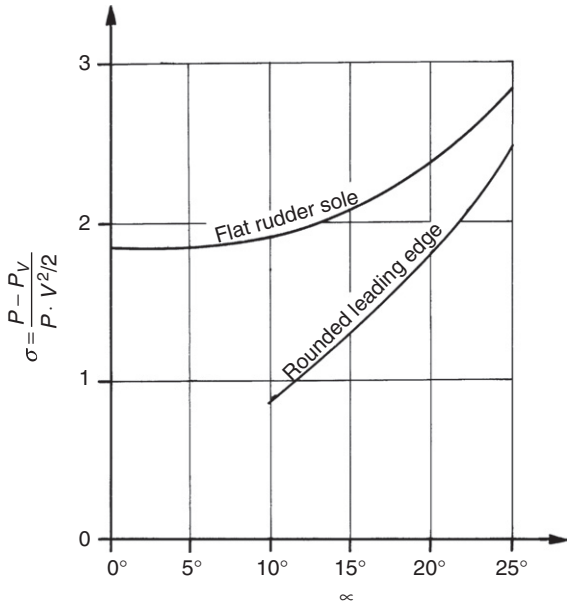

Figure 6.24:
Cavitation number *B* below which rudder sole cavitation occurs as a function of the angle of attack and the rudder sole construction

Therefore, cavitation erosion frequently occurs at the rudder at the upper and sometimes lower slipstream boundaries, mainly (for right-turning propellers) on the upper starboard side of the rudder. This problem is not confined to high-speed ships. The best means to reduce these effects is to decrease gradually the propeller loading to the blade tips by appropriately reduced pitch, and to use a high propeller skew. These methods also reduce propeller-induced vibrations.

4. *Propeller hub cavitation*
   Behind the propeller hub a vortex is formed which is often filled by a cavitation tube. However, it seems to cause fewer problems at the rudder than the tip vortices, possibly due to the lower axial velocity behind the propeller hub.
5. *Cavitation at surface irregularities*
   Surface irregularities disturbing the smooth flow cause high flow velocities at convex surfaces and edges, correspondingly low pressures, and frequently cavitation erosion. At the rudder, such irregularities may be zinc anodes and shaft couplings. It is reported that also behind scoops, propeller bossing, etc. cavitation erosion occurred, possibly due to increased turbulence of the flow. Gaps between the horn and the rudder blade in semi-balanced rudders are especially prone to cavitation, leading to erosion of structurally important parts of the rudder. For horizontal and vertical gaps (also in flap rudders) the rounding of edges of the part behind the gap is recommended.

6.4.7. Rudder Design

There are no regulations for the rating of the rudder area. The known recommendations give the rudder area as a percentage of the underwater lateral area $L \cdot T$. Det Norske Veritas recommends:

$$\frac{A_R}{L \cdot T} \geq 0.01 \cdot \left(1 + 25\left(\frac{B}{L}\right)^2\right) \tag{6.91}$$

This gives a rudder area of approximately 1.5% of the underwater lateral area for ships of usual width; for unusually broad ships (large mass, low yaw stability) a somewhat larger value is given. This corresponds to typical rudder designs and can serve as a starting point for further analyses of the steering qualities of a ship.

Recommended minimum criteria for the steering qualities of a ship are:

- Non-dimensional initial turning time in Z 20°/10° maneuvers: $t'_a = 1 + 1.73F_n$.
- Non-dimensional yaw checking time in Z 20°/10° maneuvers: $t'_s = 0.78 + 2.12F_n$.
- The rudder should be able to keep the ship on a straight course with a rudder angle of maximum 20° for wind from arbitrary direction and $v_w/V = 5$. v_w is the wind speed, V the ship speed.
- The ship must be able to achieve a turning circle of less than $5 \cdot L$ at the same v_w/V for maximum rudder angle.

The criteria for initial turning time and yaw checking time were derived by Brix using regression analysis for 20°/10° zigzag test results for many ships (Fig. 6.8). The time criteria are critical for large ships (bulkers, tankers), while the wind criteria are critical for ships with a large lateral area above the water (ferries, combatants, container ships). An additional criterion concerning yaw stability would make sense, but this would be difficult to check computationally.

The rudder design can be checked against the above criteria using computations (less accurate) or model tests (more expensive). A third option would be the systematically varied computations of Wagner, described in Brix (1993, pp. 95−102). This approach yields a coefficient $C_{Y\delta}$ for rudder effectiveness which inherently meets the above criteria. The method described in Brix (1993) uses design diagrams. For computer calculations, empirical formulae also derived by Wagner exist.

6.4.8. CFD for Rudder Flows and Conclusions for Rudder Design

The determination of forces on the rudder is important for practical design purposes:

- The transverse force is needed to evaluate the maneuverability of ships already in the design stage as required by IMO.
- The longitudinal force influences noticeably the propulsive efficiency.
- The shaft torsional moment is decisive for selecting a suitable rudder gear.

In principle, there are three sources of information for these forces:

- Model experiments which produce accurate forces at model Reynolds numbers, but suffer from severe scale effects when predicting the maximum lift at full scale.
- RANSE computations appear to be the most reliable source of information and should gain in importance also for practical design of rudders.
- BEM computations can often give sufficiently accurate results with a minimum of effort if some empirical relationships and corrections are applied.

Söding (1998a, b) described the state of the art for BEM comparing the results to RANSE and experimental results. The RANSE computations used for comparison were finite-volume methods employing a standard $k-\varepsilon$ turbulence model with wall function.

Söding's BEM approach for rudder flows introduces some special features:

- Special adaptations of the BEM take the irrotational inflow to the rudder induced by hull and propeller into account.
- The propeller slipstream is averaged in the circumferential direction. The radial thrust distribution is assumed such that it approaches gradually zero at the outer limit and is zero in the hub region.
- The ship hull above the rudder can either be modeled as horizontal mirror plane or as a separate body discretized by boundary elements.

The BEM results were compared to RANSE and experimental results for various rudders. According to potential theory, a thin foil in two-dimensional flow (i.e. for aspect ratio $\Lambda = \infty$) at a small angle of attack α produces lift nearly linearly increasing with α corresponding to:

$$\frac{\mathrm{d}C_L}{\mathrm{d}\alpha} = 2\pi \tag{6.92}$$

In three-dimensional flow, the lift gradient is decreased by a reduction factor $r(\Lambda)$ *w*hich is well approximated by:

$$r(\Lambda) = \Lambda\frac{\Lambda + 0.7}{(\Lambda + 1.7)^2} \tag{6.93}$$

Except for Λ, details of the rudder shape in side view (e.g. rectangular or trapezoidal) have hardly any influence on $\mathrm{d}C_L/\mathrm{d}\alpha$. However, the profile thickness and shape have some influence. Computations and measurements of the lift coefficient corrected for infinite aspect ratio by the formula above yield the following conclusions:

- All values differ from the theoretical value 2π by less than $\pm 17\%$.
- For the same profile, measurements and computations by any method differ generally by only a few per cent, except for NACA profiles with thickness ratio greater than 25%.
- Two-dimensional and three-dimensional RANSE computations hardly differ from each other except for thick NACA profiles.

- The Reynolds number based on axial inflow velocity and mean rudder chord length has relatively little effect on the lift gradient.
- The BEM fails to predict the low lift gradient of profiles with large opening angle of the trailing edge. For such profiles, the Kutta condition used in potential flow is a poor approximation.
- Substantial thickness at the trailing edge increases the lift slope.

Further detailed investigations based on RANSE computations produced the following insight into the effect of profile thickness:

- Thick profiles produce more lift than thinner ones if they have a sharp end (concave sides), and a lower lift if they end in a larger angle (convex or flat sides).
- The mostly used NACA00 profiles are worse than the other profiles investigated, both with respect to lift slope and to the ratio between lift and drag.
- For all profiles, the lift/drag ratio decreases with increasing thickness. Therefore, for a good propulsive efficiency, one should use the thinnest possible profile.
- The IFS profile generates the largest lift. However, when compared to the HSVA MP73-25 profile the difference is small and the lift/drag ratio is worse than for the HSVA profile. The IFS profile is also more liable to suffer from cavitation due to its very uneven pressure distribution on the suction side.

BEM is not capable of predicting the stall angle because stall is inherently a viscous phenomenon. For hard-over maneuvers, the stall angle and its associated maximum lift may be more important than $\mathrm{d}C_L/\mathrm{d}\alpha$. RANSE computations show that higher Reynolds numbers produce larger maximum C_L. Thus experimental values without extrapolation to actual Reynolds numbers are misleading with respect to maximum lift forces. Other conclusions for the maximum lift at stall angle from RANSE computations are:

- The maximum C_L ranges between 1.2 and more than 2. This upper limit is substantially larger than assumed in classification rules.
- The aspect ratio Λ is of minor influence only. Larger aspect ratio produces somewhat smaller $C_{L,\max}$.
- Small Λ yield large stall angles. (They also yield small $\mathrm{d}C_L/\mathrm{d}\alpha$, hence little change in the maximum C_L.)
- The taper ratio of the rudder has practically no influence on the maximum C_L.
- Profiles with concave sides produce larger $C_{L,\max}$ than those with flat or convex sides.

Three-dimensional RANSE computations give slightly lower maximum C_L than two-dimensional RANSE computations. The relation between the two-dimensional and three-dimensional values approximately determines the maximum lift while avoiding the complexities (and cost) of three-dimensional RANSE computations, especially for complex configurations and non-uniform inflow.

The recommended procedure is then:

- Perform a two-dimensional RANSE computation for the actual profile and Reynolds number in uniform flow to determine the maximum C_L.
- Perform a panel calculation for the three-dimensional arrangement.
- Convert the computed lift to C_L using an average inflow velocity. The averaged velocity is the root mean square axial velocity averaged over the rudder height.
- Determine the approximate stall angle as that where the three-dimensional C_L in potential flow amounts to 95% of the maximum $C_{L,2d}$ in the two-dimensional RANSE computation.
- Truncate the computed lift forces at that angle, but not drag and stock moment.

In practice, the aftbody arrangement with propeller and rudder is rather more complicated and may even involve additional complexities such as nozzles, fins, and bulbs. These make grid generation for field methods (and even BEM) complicated. However, by 2010 RANSE simulations for hull−propeller−rudder interaction at full-scale Reynolds numbers started to drift into industry applications.